D

Debye-Hückel Equation

Jay R. Black
School of Earth Sciences, The University of Melbourne, Melbourne, VIC, Australia

Definition

Named after Peter Debye (1884–1966) and Erich Hückel (1896–1980) for their work pioneering the understanding of aqueous electrolyte solutions, the Debye-Hückel equation defines the activity coefficient (γ) of an aqueous ion as a function of the ionic strength of solution. Models that incorporate Debye-Hückel's theory and equations enable geochemists to predict the complex speciation of solutes in aqueous solutions from thermodynamic principles (See ▶ "Activity and Activity Coefficients"; ▶ "Aqueous Solutions"; ▶ "Complexes"; ▶ "Geochemical Thermodynamics").

Debye-Hückel Models

There are a number of theoretical expressions of the Debye-Hückel model, the primitive Debye-Hückel model describes long-range Coulombic forces between dissolved ions where the solvent acts as a structureless dielectric continuum and solutes are defined as hard spheres with a charge at the center (See "Electrolyte Theory"). Coulombic interactions between dissolved ions tend to promote ordering of negatively charged anions around positively charged cations, and vice versa, leading to a decrease in the thermodynamic free energy of the system (See ▶ "Free Energy") compared to if the dissolved ions were distributed randomly in solution. If ions are considered to be point charges then Coulombic interactions between ions will lead to a Boltzmann distribution of ions around one another and the Debye-Hückel limiting law is defined as:

$$\log_{10}\gamma_i = -Az_i^2\sqrt{I} \quad (1)$$

where A is a constant that is dependent on temperature and pressure, z_i is the charge on the ion (i) and I is the ionic strength defined by the equation:

$$I = \frac{1}{2}\sum_i m_i z_i^2 \quad (2)$$

where, m_i is the molal concentration of the ion (i). Equation 1 is only valid for very low ionic strengths ($I < 10^{-3}$ molal) due to the assumption of ions being point charges. The Debye-Hückel model can be extended to higher ionic strengths by considering that ions have a finite diameter, yielding the equation:

$$\log_{10}\gamma_i = \frac{-Az_i^2\sqrt{I}}{1 + B\mathring{a}\sqrt{I}} \quad (3)$$

where B is a constant that is dependent on temperature and pressure and $\mathring{a}$ is the distance of closest approach equivalent to the hydrated radius of the ion in Angstroms.

Equation 3 is generally valid for $I <= 0.1$ molal for monovalent ions, but lower ionic strengths for multi-valent ions and mixed electrolyte solutions. The parameter $\mathring{a}$ can be varied for different ionic species, as would be expected due to different ionic complexes having different hydrated radii, however doing so violates the assumption of the Debye-Hückel model that all ions are hard-spheres of the same diameter and thermodynamic relationships can no longer be satisfied (See ▶ "Geochemical Thermodynamics"). As such, some variations of Eq. 3 assume the $B\mathring{a}$ term is constant regardless of ion type, e.g., where $B\mathring{a} = 1$ it is known at the Güntelberg equation. Varying $\mathring{a}$ for different ions is often used in the implementation of the Debye-Hückel model in various thermodynamic databases for geochemical modeling programs (e.g., WATEQ: Truesdell and Jones 1974; EQ3/6: Wolery and Jarek 2003).

W. M. White (ed.), *Encyclopedia of Geochemistry*,
https://doi.org/10.1007/978-3-319-39312-4

At higher ionic strengths the primitive Debye-Hückel models become inaccurate due a number of effects and underlying assumptions. Real solutes are not hard-spheres with a central charge and the hydration state of ions can change with increasing ionic strength and vary between different ionic complexes (i.e., different values for $\mathring{a}$). Ion association (See ▶ "Complexes") becomes increasingly important at higher ionic strengths and hard-core effects become important (Pitzer 1973). Attempts to expand the Debye-Hückel model further to account for ion association at higher ionic strengths have included an extra ionic strength dependent term:

$$\log_{10}\gamma_i = \frac{-Az_i^2\sqrt{I}}{1 + B\mathring{a}\sqrt{I}} + bI \quad (4)$$

where b is a constant that may or may not be ion specific. Various expansions of the Debye-Hückel equation of this nature are collectively referred to as specific ion interaction theory, one form of which is the Davies (1962) equation.

Care must be taken when computing the value for the constant A depending upon whether the form of the Debye-Hückel model being used is written as ln γ or $\log_{10}\gamma$ and similarly care must be taken with the units of the constant A being on the same length scale used for parameter $\mathring{a}$. Analytical expressions for the constants A and B from 25 °C to 600 °C and 0.001–5 kbar pressure can be found in Helgeson and Kirkham (1974).

Model Comparison to Experiments

Activity coefficients for individual ions cannot be measured, as such, measured values for the mean activity coefficient of NaCl (γ_{NaCl}) at various ionic strengths are plotted in Fig. 1 (Robinson and Stokes 1965; Haynes 2015–2016) and compared to calculations using the Debye-Hückel models presented here (Eqs. 1, 2, 3, and 4). Since Eqs. 1, 3 and 4 calculate activity coefficients for individual ionic species (Na^+ and Cl^-), the mean activity coefficient is determined using the following equation:

$$\gamma_{NaCl} = \sqrt{\gamma_{Na^+}\gamma_{Cl^-}} \quad (5)$$

At high enough dilutions Debye-Hückel models fit measured activity coefficients for solutes very well, however, the monotonic decrease of the activity coefficient predicted by Eqs. 1 and 3 with increasing ionic strength is no longer observed in solutions of high ionic strength ($I >$ c. 1.2 molal) where the activity coefficient exponentially increases (Fig. 1). Debye-Hückel models such as that presented in Eq. 4 can be empirically fit to experimental data (e.g., Fig. 1).

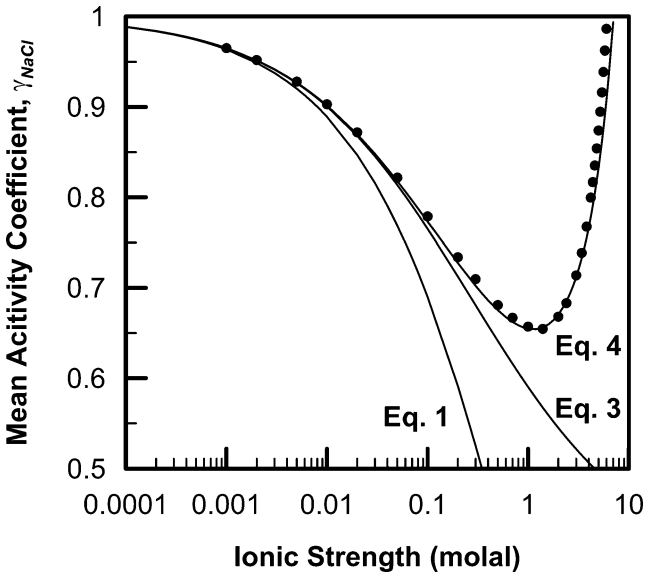

Debye-Hückel Equation, Fig. 1 Mean activity coefficients for NaCl at 25 °C as a function of ionic strength. Experimental data plotted as circles (Robinson and Stokes 1965; Haynes 2015–2016). Results using Eqs. 1, 2, 3, and 4 and with Eq. 5 are plotted as lines using: $\mathring{a}_{Na} = 4$; $\mathring{a}_{Cl} = 3.5$; $b_{Na} = 0.075$; $b_{Cl} = 0.015$ (Truesdell and Jones 1974)

Summary and Conclusion

The Debye-Hückel equation and models derived from the underlying electrolyte theory allow geochemists to model the behavior of ionic solutes in dilute aqueous solutions. The expanded version of the Debye-Hückel equation presented in Eq. 4 fits experimental data for NaCl up to much higher ionic strengths (close to the solubility limit for NaCl, Fig. 1). However, the most successful specific ion interaction theory models expanding on the Debye-Hückel equation are those of Pitzer (1973). Pitzer's equations account for secondary and tertiary ion-pair interactions through a virial expansion of the Debye-Hückel model and can successfully model systems containing single and multiple electrolytes to high ionic strengths. For further reading see Pitzer (1973) and implementation of the Pitzer equations to geochemical modeling (Wolery and Jarek 2003).

Cross-References

- ▶ Activity and Activity Coefficients
- ▶ Aqueous Solutions
- ▶ Complexes
- ▶ Free Energy
- ▶ Geochemical Thermodynamics

References

Davies CW (1962) Ion association. Butterworths, London. 190 pp
Haynes WM (2015–2016) CRC handbook of chemistry and physics, 96th edn. Taylor and Francis GroupLLC, Boca Raton
Helgeson HC, Kirkham DH (1974) Theoretical prediction of the thermodynamic behavior of aqueous electrolytes at high pressures and temperatures: II. Debye-Hückel parameters for activity coefficients and relative partial molal properties Am J Sci 274:1199–1261
Pitzer KS (1973) Thermodynamics of electrolytes. I. Theoretical basis and general equations. J Phys Chem 77:268–277
Robinson RA, Stokes RH (1965) Electrolyte solutions, 2nd edn., revised. Butterworths, London. 571 pp
Truesdell AH, Jones BF (1974) WATEQ, a computer program for calculating chemical equilibria of natural waters. J Res US Geol Surv 2:233–248
Wolery TW, Jarek RL (2003) Software User's manual EQ 3/6, Version 8.0. Sandia National Laboratories/U.S. Department of Energy Report. 376 pp

Density Functional Theory

David A. Dixon
Department of Chemistry, University of Alabama, Tuscaloosa, AL, USA

Definition

Density functional theory is an approach to solving the Schrödinger equation for the motion of electrons in molecules (as well as atoms) based on the concept that the energy is a functional of the density. In principle, it is an exact theory if the density and the functional are known. In practice, the exact form of the functional is not known. This method is another way to solve the Schrödinger equation for the electronic motion of electrons in atoms and molecules in addition to molecular orbital theory. It has been extensively applied to both molecules and solids and is probably the most common method in use today for electronic structure calculations.

Overview

Density functional theory (DFT) can be used to determine the ground state energy of the system as well as to predict a wide range of properties including structures, spectra, energetics, and charge distributions (Parr and Wang 1989; Dreizler and Gross 1990; Labanowski and Andzelm 1991; Seminario and Politzer 1995; Laird et al. 1996; Springborg 1997; Sholl and Steckel 2009). Rather than solving the Schrödinger equation explicitly as in molecular orbital theory, one uses a theorem (Hohenberg and Kohn 1964) which states that the exact energy is a functional of the density ρ. This means there is a one-to-one correspondence between the electronic energy and the electron density. The foundation for the use of DFT methods in computational geochemistry was the realization that the external potential is determined, within an additive constant, by the electron density (Kohn and Sham 1965). Since the wave function is a functional of the electron density, it follows that the density also determines the ground state wave function and all other electronic properties of the system. Because ρ determines N (the number of electrons) and v (the external potential) and hence all the properties of the electronic ground state, we can write the energy to explicitly depend on v:

$$E_v[\rho] = T[\rho] + V_{ne}[\rho] + V_{ee}[\rho] = \int \rho(r)v(r)dr + F_{HK}[\rho] \quad (1)$$

where

$$F_{HK}[\rho] = T[\rho] + V_{ee}[\rho] \quad (2)$$

We write $V_{ee}[\rho] = J[\rho] + E_{xc}[\rho]$, where $J[\rho]$ is the classical repulsion and $E_{xc}[\rho]$ is a nonclassical term referred to as the "exchange-correlation energy." The first and second terms correspond to the kinetic energy of the electrons and to the classical Coulomb electronic-nuclear attraction term, respectively. The $E_{ne}[\rho]$ and $J[\rho]$ terms are given by their classical expressions (Eqs. 3 and 4), and the factor of ½ in the $J[\rho]$ functional allows for the integration over all space for both variables:

$$E_{ne}[\rho] = \sum_a \int \frac{Z_a \rho(r)}{|R_a - r|} dr \quad (3)$$

$$J[\rho] = \frac{1}{2} \iint \frac{\rho(r)\rho(r')}{|r - r'|} dr dr' \quad (4)$$

The last term, E_{xc} the exchange-correlation energy, contains all of the many-body contributions to the energy. If the form of this term were known exactly, then one could solve for the total energy using Eq. 1, but, the exact form of this term is not known, so it is necessary to use some approximation for E_{xc}. The last term contains the exchange energy $K[\rho]$ and the correlation energy. For a noninteracting uniform electron gas, $T[\rho]$ and $K[\rho]$ are given by Eqs. 5 and 6:

$$T[\rho] = C_F \int \rho^{\frac{5}{3}}(r) dr \quad (5)$$

$$K[\rho] = -C_x \int \rho^{\frac{4}{3}}(r) dr \quad (6)$$

with the coefficients C_F and C_x given by

$$C_F = \frac{3}{10}\left(3\pi^2\right)^{\frac{2}{3}} \tag{7}$$

$$C_x = \frac{3}{4}\left(\frac{3}{\pi}\right)^{\frac{1}{3}} \tag{8}$$

The second Hohenberg-Kohn theorem provides the energy variational principle, $E_0[\rho_0] < \mathrm{E}_0[\rho]$ for $\rho_0 \neq \rho$; the exact energy for the ground state is obtained for $\rho_0 = \rho$. This is analogous to the variational principle for wave functions from molecular orbital theory.

Although DFT has been around since the mid-1960s, it is only recently (since ~ 1990) that its application to chemical, including geochemical, problems has become popular. This was because of the development of new approaches to solve the DFT equations implemented in software used by chemists coupled with exchange-correlation functionals that could be applied for use in chemical molecular problems. In addition, DFT works very well for many chemical systems with a reduced computational cost. For about the same cost of doing a Hartree-Fock calculation, DFT usually includes a significant fraction of the electron correlation energy. Note that DFT is *not* a Hartree-Fock method, nor is it (strictly speaking) a post-Hartree-Fock method. The wave function is constructed in a different way (the spin and spatial parts are different to those developed in Hartree-Fock theory), and the resulting orbitals are often referred to as "Kohn-Sham" orbitals.

The computer programs that actually solve the DFT equations have much in common with Hartree-Fock electronic structure programs, and chemical theorists initially adapted their Hartree-Fock programs to perform DFT computations, although there were a number of codes that were developed just for DFT. Like Hartree-Fock, the DFT equations must be solved self-consistently, making DFT another type of self-consistent field (SCF) method. Instead of focusing on wave functions and orbitals, DFT focuses on the electron density, although molecular DFT calculations usually employ orbitals to get the density. As it includes an approximate treatment of electron correlation, it should be more accurate than Hartree-Fock theory. There are many different variations of DFT, depending on the particular treatment of correlation and exchange, i.e., the choice of the exchange-correlation functional. The main drawback of DFT is that as the exact form of the exchange-correlation functional is not known, improvements to the functional are not straightforward. This contrasts with other *ab initio* electronic structure methods, where one can keep improving the results until the electronic Schrödinger equation is solved exactly. The reason DFT is broadly used is that it tends to give very accurate results much more cheaply than many competing MO-based methods, especially for molecules containing transition metals.

Functionals

The two input computational parameters for the solution of the Schrödinger equation for a system using DFT are the exchange-correlation functional and the functions used to represent the electrons, the one-particle basis set. At the present time, there is no formal systematic way of choosing the functional, and the most popular ones in the literature have been derived by careful comparison with experiment as well as meeting the formal criteria for a functional (Scuseria and Staroverov 2005). Examples of commonly used functionals are given in Table 1. The selected examples of DFT exchange-correlation functionals consist of (1) local spin density approximation (LSDA), (2) generalized gradient approximations (GGA), (3) meta GGA (mGGA), (4) hybrid GGA (HGGA), and (5) hybrid meta GGA (HmGGA) functionals. We note that Perdew and coworkers have called the hierarchy of functionals the "Jacob's ladder of functionals"(Perdew and Schmidt 2001; Tao et al. 2003; Perdew et al. 2005). The first level of approximation usually used is the local density approximation, and this is usually taken as Slater exchange together with the correlation energy of the uniform electron gas. This functional depends only on the density. The LSDA for the exchange-correlation functional in DFT is well known for its accuracy in predicting properties such as lattice parameters and bulk moduli in metallic systems. However, the LSDA results for electronic properties are of lower quality, because of intrinsic deficiencies, including missing self-interaction corrections and the absence of the derivative discontinuity in the exchange-correlation potential.

The functional can be improved by incorporating gradient (nonlocal) corrections to the exchange and correlation energy (GGA). A third type of functional, called hybrid GGA (HGGA), is a gradient-corrected functional that includes some components of HF exact exchange. For molecules, hybrid exchange-correlation functionals often show improvement in the prediction of energetics over those from GGA functionals because the hybrid functionals help to delocalize the exchange hole. Hybrid functionals have proven to be equally good at predicting a range of physical properties, but such calculations in the solid state are computationally expensive due to the need to calculate Hartree-Fock exchange (Kudin et al. 2002). Commonly used GGAs are B88P86, PBE, and PW91. B3LYP is the most commonly used HGGA by a wide margin.

Weak interactions such as those involving van der Waals interactions or hydrogen bonding are important for geochemical applications. As hydrogen bonding has some electrostatic

Density Functional Theory, Table 1 Selected DFT exchange-correlation functionals

Method	Exchange	Correlation	Type
B1B95	(Becke 1996)	(Becke 1996)	HmGGA
B1LYP Adamo and Barone 1997	(Becke 1996)	Lee-Yang-Parr (Lee et al. 1988)	HGGA
B3LYP	(Becke 1993)	Lee-Yang-Parr (Lee et al. 1988)	HGGA
B972	Wilson-Bradley-Tozer's modified B97 (Wilson et al. 2001)	Wilson-Bradley-Tozer's modified B97 (Wilson et al. 2001)	HGGA
B98	Becke 98 (Schmider and Becke 1998)	Becke 98 (Schmider and Becke 1998)	HGGA
BLYP	(Becke 1988)	Lee-Yang-Parr (Lee et al. 1988)	GGA
BMK	(Boese and Martin 2004)	(Boese and Martin 2004)	HGGA
B88P86	(Becke 1988)	(Perdew 1986)	GGA
CAMB3LYP (Yanai et al. 2004)	(Becke 1988)	Lee-Yang-Parr (Lee et al. 1988)	HGGA[a]
G96LYP	Gill 1996	Lee et al. 1988	GGA
HCTH407	Hamprecht, Cohen, Tozer, Hand (Hamprecht et al. 1998) (Boese et al. 2000) (Boese and Handy 2001)	Hamprecht, Cohen, Tozer, Hand (Hamprecht et al. 1998) (Boese et al. 2000) (Boese and Handy 2001)	GGA
HSE1PBE	Heyd-Scuseria-Ernzerhof (Heyd et al. 2003, 2005) (Heyd and Scuseria 2004) (Krukau et al. 2006)	Perdew-Burke-Ernzerhof (Perdew et al. 1996)	HGGA
LCBP86 (Iikura et al. 2001)	(Becke 88)	(Perdew 1986)	GGA[a]
LCωPBE (Vydrov and Scuseria 2006)	Perdew-Burke-Ernzerhof (Perdew et al. 1996)	Perdew-Burke-Ernzerhof (Perdew et al. 1996)	HGGA[a]
M06	Minnesota 06 (Zhao and Truhlar 2008)	Minnesota 06 (Zhao and Truhlar 2008)	HmGGA
mPW1PW91	Barone's modified PW91 (Adamo and Barone 1998)	Perdew-Wang 91 (Perdew and Wang 1992)	HGGA
O3LYP/OLYP	Handy's OPTX (Cohen and Handy 2001; Handy and Cohen 2001)	Lee-Yang-Parr (Lee et al. 1988)	HGGA/ GGA
PBE/PBE1PBE	Perdew-Burke-Ernzerhof (Perdew et al. 1996)	Perdew-Burke-Ernzerhof (Perdew et al. 1996)	GGA/HGGA
PBEhPBE/PBEh1PBE	98 Revised PBE (Ernzerhof and Perdew 1998)	Perdew-Burke-Ernzerhof (Perdew et al. 1996)	GGA/ HGGA
PKZB	Perdew, Kurth, Zupan, Blaha (Perdew et al. 1999)	Perdew, Kurth, Zupan, Blaha (Perdew et al. 1999)	GGA
PW91	Perdew-Wang 91 (Perdew and Wang 1992; Burke et al. 1997)	Perdew-Wang 1991 (Perdew and Wang 1992)	GGA
SVWN5	(Slater 1974)	VWN functional (Vosko et al. 1980)	LSDA
τ-HCTH(hyb)	τ-dependent of HCTH (Boese and Handy 2002)	τ-dependent of HCTH (Boese and Handy 2002)	mGGA (HGGA)
TPSS	Tao-Perdew-Staroverov-Scuseria (Tao et al. 2003)	Tao-Perdew-Staroverov-Scuseria (Tao et al. 2003)	mGGA
TPSSh	Tao-Perdew-Staroverov-Scuseria (Staroverov et al. 2003)	Tao-Perdew-Staroverov-Scuseria (Staroverov et al. 2003)	HmGGA
VSXC	(van Voorhis and Scuseria 1997, 1998)	(van Voorhis and Scuseria 1997, 1998)	mGGA
ωB97(X, X-D) (Chai, Head-Gordon, 2008)	(Becke 1997)	(Becke 1997)	HGGA[a]
X3LYP (Xu and Goddard 2004)	(Becke 1988) (Perdew-Wang 1992)	Lee-Yang-Parr (Lee et al. 1988)	HGGA

[a]Long range corrected exchange correlation functional.

D

or dipolar component, a number of functionals can provide reasonable hydrogen bond energies, although if there are a large number of such interactions, the total error may not be small. On the other hand, most common DFT functionals do not handle dispersion corrections properly. One approach is to add in a set of atom-pairwise empirically based corrections as developed by Grimme and coworkers, the –D3 correction, for example (Grimme 2006; Grimme et al. 2010). Another approach is to add on a more formally developed correction based on the electron density a van der Waals nonlocal functional, which is added to commonly used exchange and correlation components, such as the VV10 functional (Vydrov and Van Voorhis 2009, 2010). These different types of corrections have been evaluated (Hujo and Grimme 2011, 2013; Mardirossian and Head-Gordon 2014).

The use of approximate exchange-correlation functionals allows one to solve the density functional equation exactly for an approximate energy expression, whereas molecular orbital methods solve an exact expression for the energy approximately. An advantage of many DFT functionals without exact exchange is that they formally scale as N^3 as compared to the N^4 scaling of Hartree-Fock theory and the N^5–N^7 scaling of common correlation methods. Thus, DFT methods, if derived without the inclusion of Hartree-Fock exchange, are computationally much cheaper than Hartree-Fock-based methods and exhibit a much better scaling with the size of the molecule. In fact, the Hartree-Fock method is a special case of DFT with the exchange term computed exactly and the correlation term equal to zero.

Other Features of DFT

An important use of DFT is to predict spectroscopic properties. The prediction of infrared and Raman vibrational spectra including intensities for molecules follows the second derivative methods developed for molecular orbital theory. UV-vis spectra can be calculated using time-dependent density functional theory (TD-DFT) (Bauernschmitt and Ahlrichs 1996; Casida et al. 1998). Nuclear magnetic resonance chemical shifts can be calculated using the gauge invariant atomic orbital (GIAO) approach (Wolinski et al. 1990) with density functional theory (Schreckenbach and Ziegler 1995, 1996, 1997). It is also possible to include relativistic effects in the zeroth-order regular approximation (ZORA) for the NMR chemical shifts (Wolff and Ziegler 1998; Wolff et al. 1999; Autschbach and Ziegler 2004).

As DFT developed as a broad-based chemical tool for predicting structures and energetics, there has been a continued development of the method for providing insights into chemical bonding and reactivity. This approach is often called conceptual DFT (Geerlings et al. 2003, 2014; De Proft et al. 2014). For example, it provides formal definitions of hardness and softness, the basis of hard-soft acid/base theory as well as electronegativity.

Solid State and Plane Waves

DFT calculations on solids are done with periodic boundary conditions. Plane waves are usually used rather than the Gaussian-type orbitals used in molecular calculations although the latter can be used in solid-state calculations. Plane waves are used in the electronic structure because they fit more naturally with the Bloch states and they are expanded in Wannier functions. In addition, they do not have the problems that Gaussian orbitals have in calculating diffuse parts of the wave function. The periodic calculations can be performed using the projector augmented wave (PAW) method, which deals with the full wave functions and allows the treatment of all elements in the periodic table (Blöchl 1994). Such calculations usually employ pseudopotentials so that calculations are only performed on the valence electrons as the contracted size of the inner shell orbitals makes it difficult to calculate these electronic states using plane waves. Ultrasoft pseudopotentials (Vanderbilt 1990) are broadly used and, for example, allow first-row transition metal elements to be dealt with in an economical manner.

Several approaches to improving the quality of band gaps including LSDA + U, which relies on LSDA-optimized lattice parameters, and many-body perturbation theory in the framework of the Green's function (GW) method have been developed (Grossman et al. 2001; Onida et al. 2002). Although these approaches predict improved band gaps, just like hybrid functionals, they are computationally demanding and are usually applied only to small systems. By using a screened hybrid functional that includes nonlocal Hartree-Fock exchange but decomposes the Coulomb operator into short-range and long-range components, such as that in the HSE functional (Heyd et al. 2003), it is possible to accurately and efficiently predict semiconductor and insulator band gaps (Prodan et al. 2007).

Conclusions

Density functional theory is an important tool for predicting the properties of geochemical systems based on their electronic structure. It is important to choose a properly benchmarked exchange-correlation functional together with an appropriate basis set. DFT can provide a broad

range of structural, energetic, and spectroscopic predictions that can be used to obtain detailed insights into geochemical systems at the molecular level. DFT is currently the most popular computational electronic structure method for geochemical applications, especially for predictions in the solid state or at extended interfaces. DFT can also provide qualitative insights into molecular reactivity through the use of conceptual DFT.

Cross-References

► Ab Initio Calculations

References

Adamo C, Barone V (1997) Toward reliable adiabatic connection models free from adjustable parameters. Chem Phys Lett 274:242–250

Adamo C, Barone V (1998) Exchange functionals with improved long-range behavior and adiabatic connection methods without adjustable parameters: the mPW and mPW1PW models. J Chem Phys 108:664–675

Autschbach J, Ziegler T (2004) Calculation of heavy-nucleus chemical shifts: relativistic all-electron methods. In: Kaupp M, Buhl M, Malkin VG (eds) Calculation of NMR and EPR parameters: theory and application. Wiley-VCH & Co, Weinheim, pp 249–264

Bauernschmitt R, Ahlrichs R (1996) Treatment of electronic excitations within the adiabatic approximation of time dependent density functional theory. Chem Phys Lett 256:454–464

Becke AD (1988) Density-functional exchange-energy approximation with correct asymptotic behavior. Phys Rev A 38:3098–3100

Becke AD (1993) Density-functional thermochemistry. III. The role of exact exchange. J Chem Phys 98:5648–5652

Becke AD (1996) Density-functional thermochemistry. IV. A new dynamical correlation functional and implications for exact-exchange mixing. J Chem Phys 104:1040–1046

Becke AD (1997) Density-functional thermochemistry. V. Systematic optimization of exchange-correlation functionals. J Chem Phys 107:8554–8560

Blöchl PE (1994) Projector augmented-wave method. Phys Rev B 50:17953–17979

Boese AD, Handy NC (2001) A new parametrization of exchange-correlation generalized gradient approximation functionals. J Chem Phys 114:5497–5503

Boese AD, Handy NC (2002) New exchange-correlation density functionals: the role of the kinetic-energy density. J Chem Phys 116:9559–9969

Boese AD, Martin JML (2004) Development of density functionals for thermochemical kinetics. J Chem Phys 121:3405–3416

Boese AD, Doltsinis NL, Handy NC, Sprik M (2000) New generalized gradient approximation functionals. J Chem Phys 112:1670–1678

Burke K, Perdew JP, Wang Y (1997) Derivation of a generalized gradient approximation: the PW91 density functional. In: Dobson JF, Vignale G, Das MP (eds) Electronic density functional theory: recent progress and new directions. Plenum, New York, pp 81–121

Casida ME, Jamorski C, Casida KC, Salahub DR (1998) Molecular excitation energies to high-lying bound states from time-dependent density-functional response theory: characterization and correction of the time-dependent local density approximation ionization threshold. J Chem Phys 108:4439–4449

Chai J-D, Head-Gordon M (2008) Systematic optimization of long-range corrected hybrid density functionals. J Chem Phys 128:084106. (15pages)

Cohen AJ, Handy NC (2001) Dynamic correlation. Mol Phys 99:607–615

De Proft F, Ayers PW, Geerlings P (2014) Chapter. 7. The conceptual density functional theory perspective of bonding. In: Frenking G, Shaik S (eds) The chemical bond: fundamental aspects of chemical bonding. Wiley, New York, pp 233–265

Dreizler RM, Gross EKU (1990) Density functional theory. An approach to the quantum many-body problem. Springer, Berlin

Ernzerhof M, Perdew JP (1998) Generalized gradient approximation to the angle- and system-averaged exchange hole. J Chem Phys 109:3313–3320

Geerlings P, De Proft F, Langenaecker W (2003) Conceptual density functional theory. Chem Rev 103:1793–1873

Geerlings P, Fias S, Boisdenghien Z, De Proft F (2014) Conceptual DFT: chemistry from the linear response function. Chem Soc Rev 43:4989–5008

Gill PMW (1996) A new gradient-corrected exchange functional. Mol Phys 89:433–445

Grimme S (2006) Semiempirical GGA-type density functional constructed with a long-range dispersion correction. J Comput Chem 27:1787–1799

Grimme S, Antony J, Ehrlich S, Krieg H (2010) A consistent and accurate ab initio parametrization of density functional dispersion correction (DFT-D) for the 94 elements H-Pu. J Chem Phys 132:154104

Grossman JC, Rohlfing M, Mitas L, Louie SG, Cohen ML (2001) High accuracy many-body calculational approaches for excitations in molecules. Phys Rev Lett 86:472–475

Hamprecht FA, Cohen A, Tozer DJ, Handy NC (1998) Development and assessment of new exchange-correlation functionals. J Chem Phys 109:6264–6271

Handy NC, Cohen AJ (2001) Left-right correlation energy. Mol Phys 99:403–412

Heyd J, Scuseria GE (2004) Assessment and validation of a screened Coulomb hybrid density functional. J Chem Phys 120:7274–7280

Heyd J, Scuseria GE, Ernzerhof M (2003) Hybrid functionals based on a screened Coulomb potential. J Chem Phys 118:8207–8215. Erratum: J Chem Phys 2006, 124, 219906

Heyd J, Peralta JE, Scuseria GE, Martin RL (2005) Energy band gaps and lattice parameters evaluated with the Heyd-Scuseria-Ernzerhof screened hybrid functional. J Chem Phys 123:174101. (8 pages)

Hohenberg P, Kohn W (1964) Inhomogeneous electron gas. Phys Rev 136:B864–B871

Hujo W, Grimme S (2011) Performance of the van der Waals density functional VV10 and (hybrid) GGA variants for thermochemistry and noncovalent interactions. J Chem Theory Comput 7:3866–3871

Hujo W, Grimme S (2013) Performance of non-local and atom-pairwise dispersion corrections to DFT for structural parameters of molecules with noncovalent interactions. J Chem Theory Comput 9:308–315

Iikura H, Tsuneda T, Yanai T, Hirao K (2001) Long-range correction scheme for generalized-gradient-approximation exchange functionals. J Chem Phys 115:3540–3544

Kohn W, Sham LJ (1965) Self-consistent equations including exchange and correlation effects. Phys Rev 140:A1133–A1138
Krukau AV, Vydrov OA, Izmaylov AF, Scuseria GE (2006) Influence of the exchange screening parameter on the performance of screened hybrid functionals. J Chem Phys 125:224106. (4 pages)
Kudin KN, Scuseria GE, Martin RL (2002) Hybrid density-functional theory and the insulating gap of UO2. Phys Rev Lett 89:266402. (4 pages)
Labanowski J, Andzelm JW (eds) (1991) Density functional methods in chemistry. Springer, New York
Laird BB, Ross RB, Ziegler T (eds) (1996) Chemical applications of density functional theory, ACS symposium series, vol 629. American Chemical Society, Washington
Lee C, Yang W, Parr RG (1988) Development of the Colle-Salvetti correlation-energy formula into a functional of the electron density. Phys Rev B 37:785–789
Mardirossian N, Head-Gordon M (2014) wB97X-V: a 10-parameter, range-separated hybrid, generalized gradient approximation density functional with nonlocal correlation, designed by a survival-of-the-fittest strategy. Phys Chem Chem Phys 16:9904–9924
Onida G, Reining L, Rubio A (2002) Electronic excitations: density-functional versus many-body Green's-function approaches. Rev Mod Phys 74:601–659
Parr RG, Wang W (1989) Density-functional theory of atoms and molecules. Oxford Science, New York
Perdew JP (1986) Density-functional approximation for the correlation energy of the inhomogeneous electron gas. Phys Rev B 33:8822–8824
Perdew JP, Schmidt K (2001) Jacob's ladder of density functional approximations for the exchange-correlation energy. AIP Conf Proc 577:1–20
Perdew JP, Wang Y (1992) Accurate and simple analytic representation of the electron gas correlation energy. Phys Rev B 45:13244–13249
Perdew JP, Burke K, Ernzerhof M (1996) Generalized gradient approximation made simple. Phys Rev Lett 77:3865–3868. Errata. Phys Rev Lett 1997, 78, 1396
Perdew JP, Kurth S, Zupan A, Blaha P (1999) Accurate density functional with correct formal properties: a step beyond the generalized gradient approximation. Phys Rev Lett 82:2544–2547
Perdew JP, Ruzsinszky A, Tao J, Staroverov VN, Scuseria GE, Csonka GI (2005) Prescription for the design and selection of density functional approximations: more constraint satisfaction with fewer fits. J Chem Phys 123:062201. (9 pages)
Prodan ID, Scuseria GE, Martin RL (2007) Covalency in the actinide dioxides: systematic study of the electronic properties using screened hybrid density functional theory. Phys Rev B 76:033101. (4 pages)
Schmider HL, Becke AD (1998) Optimized density functionals from the extended G2 test set. J Chem Phys 108:9624–9631
Schreckenbach G, Ziegler T (1995) Calculation of NMR shielding tensors using gauge-including atomic orbitals and modern density functional theory. J Phys Chem 99:606–611
Schreckenbach G, Ziegler T (1996) The calculation of NMR shielding tensors based on density functional theory and the frozen-core approximation. Int J Quantum Chem 60:753–766
Schreckenbach G, Ziegler T (1997) Calculation of NMR shielding tensors based on density functional theory and a scalar relativistic Pauli-type Hamiltonian. The application to transition metal complexes. Int J Quantum Chem 61:899–918
Scuseria GE, Staroverov VN (2005) Chapter 24. Development of approximate exchange-correlation functionals. In: Dykstra CE, Frenking G, Kim KS, Scuseria GE (eds) Theory and applications of computational chemistry: the first 40 years. Elsevier, Amsterdam, pp 669–724
Seminario JM, Politzer P (eds) (1995) Modern density functional theory: a tool for chemistry. Elsevier, Amsterdam
Sholl DS, Steckel JA (2009) Density functional theory: a practical introduction. Wiley, New York
Slater JC (1974) Quantum theory of molecules and solids. McGraw-Hill, New York, p 4
Springborg M (ed) (1997) Density-functional methods in chemistry and materials science. Wiley, Chichester
Staroverov VN, Scuseria GE, Tao J, Perdew JP (2003) Comparative assessment of a new nonempirical density functional: molecules and hydrogen-bonded complexes. J Chem Phys 119:12129–12137
Tao J, Perdew JP, Staroverov VN, Scuseria GE (2003) Climbing the density functional ladder: nonempirical meta-generalized gradient approximation designed for molecules and solids. Phys Rev Lett 91:146401. (4 pages)
Vanderbilt D (1990) Soft self-consistent pseudopotentials in a generalized eigenvalue formalism. Phys Rev B 41:7892–7895
Voorhis TV, Scuseria GE (1997) Exchange energy functionals based on the density matrix expansion of the Hartree-Fock exchange term. Mol Phys 92:601–608
Voorhis TV, Scuseria GE (1998) A novel form for the exchange-correlation energy functional. J Chem Phys 109:400–410; Erratum 2008, 129, 219901
Vosko SH, Wilk L, Nusair M (1980) Accurate spin-dependent electron liquid correlation energies for local spin density calculations: a critical analysis. Can J Phys 58:1200–1211
Vydrov OA, Scuseria GE (2006) Assessment of a long range corrected hybrid functional. J Chem Phys 125:234109. (9 pages)
Vydrov OA, Van Voorhis T (2009) Nonlocal van der Waals density functional made simple. Phys Rev Lett 103:063004. (4 pages)
Vydrov OA, Van Voorhis T (2010) Nonlocal van der Waals density functional: the simpler the better. J Chem Phys 133:244103. (9 pages)
Wilson PJ, Bradley TJ, Tozer DJ (2001) Hybrid exchange-correlation functional determined from thermochemical data and ab initio potentials. J Chem Phys 115:9233–9242
Wolff SK, Ziegler T (1998) Calculation of DFT-GIAO NMR shifts with the inclusion of spin-orbit coupling. J Chem Phys 109:895–905
Wolff SK, Ziegler T, van Lenthe E, Baerends EJ (1999) Density functional calculations of nuclear magnetic shieldings using the zeroth-order regular approximation (ZORA) for relativistic effects: ZORA nuclear magnetic resonance. J Chem Phys 110:7689–7698
Wolinski K, Hinton JF, Pulay P (1990) Efficient implementation of the gauge-independent atomic orbital method for NMR chemical shift calculations. J Am Chem Soc 112:8251–8260
Xu X, Goddard WA III (2004) The X3LYP extended density functional for accurate descriptions of nonbond interactions, spin states, and thermochemical properties. Proc Natl Acad Sci USA 101:2673–2677
Yanai T, Tew D, Handy N (2004) A new hybrid exchange-correlation functional using the coulomb-attenuating method (CAM-B3LYP). Chem Phys Lett 393:51–57
Zhao Y, Truhlar DG (2008) The M06 suite of density functionals for main group thermochemistry, thermochemical kinetics, noncovalent interactions, excited states, and transition elements: two new functionals and systematic testing of four M06-class functionals and 12 other functionals. Theor Chem Accounts 120:215–241

Diagenesis

Isabel P. Montañez[1] and Laura J. Crossey[2]
[1]Department of Earth and Planetary Sciences, University of California, Davis, CA, USA
[2]Department of Earth and Planetary Sciences, University of New Mexico, Albuquerque, NM, USA

Synonyms

Diagenesis classified by setting and evolutionary stage of sedimentary basins: Eogenetic or *eodiagenesis* (near surface and shallow burial), *mesogenetic* or *mesodiagenesis* (deeper burial), and *telogenetic* or *telodiagenesis* (uplifted succession) (Choquette and Pray 1970).

Diagenesis classified by process: Syndiagenesis (biogeochemical processes at the sediment-water interface through shallow burial), *anadiagenesis* (dominantly physicochemical processes under deeper burial or orogenic conditions), and *epidiagenesis* (biogeochemical processes associated with fluid flow during uplift) (Fairbridge 1967).

Catagenesis (late, deep-burial diagenesis, referred by some as "burial metamorphism" as it incorporates the earliest stage of metamorphism).

Definition

Diagenesis is the sum total of physical, chemical, and biological processes that occur in sediments and sedimentary rocks from immediately after deposition through to the metamorphic realm. No universal definition exists for diagenesis and the term has evolved since it was defined nearly 150 years ago (de Segonzac 1968). It is generally agreed that diagenetic processes occur under Earth surface conditions (~0–30 °C and 1 bar of pressure) to temperatures of ≤250 °C and pressures of up to 2.5 kb (7 km) involving a broad range of fluid compositions from fresh water to concentrated brines (Fig. 1). Diagenesis involves both the conversion of sediments into sedimentary rock and the subsequent changes that occur prior to entering the metamorphic realm. There is no distinct boundary between the culmination of diagenesis and the onset of metamorphism nor between early diagenesis and weathering. The process of diagenetic conversion begins at the sediment-water interface in marine and terrestrial depositional sites, which have sufficient accommodation space to accumulate and preserve sediments, and continues to influence mineral and organic matter throughout its burial in sedimentary basins and associated tectonic history. Given the high reactivity of many minerals and organic matter within sediments and sedimentary rocks and the evolving nature of pore fluid temperature and chemistry, diagenesis is a continually active process with a protracted history of physical and chemical processes that lead to dissolution, chemical transformation of mineral components, precipitation of new mineral cements, and maturation of organic matter. Many resources such as coal, oil, gas, and ore deposits result from diagenetic processes.

D

The Diagenetic Cycle

The diagenetic cycle begins immediately following deposition on the ocean, lake, or channel/floodplain floor and continues through shallow- to deep-burial, and for many sediments ends with exposure above sea- or base-level where erosion, chemical weathering, and other diagenetic processes take place. Water and organic matter decomposition are the agents of diagenesis providing the fuel for the chemical and microbial processes that act on newly deposited detrital siliciclastic materials and chemically precipitated minerals, such as carbonates, amorphous silica, and evaporites (Ali et al. 2010). The course of diagenesis is dictated by sedimentary factors such as particle size and mineralogic composition, fluid-rock ratio, fluid chemistry and flow rates, organic matter content, the presence of microbial communities, as well as environmental conditions (temperature, fluid chemistry, pressure). In turn, diagenetic processes can change the chemical properties of the pore fluids over time, causing additional changes to mineralogy, fluid composition, and petrologic properties. Figure 1 summarizes many aspects of diagenesis. Figure 2 places these processes in a schematic cross section and provides a framework for the conditions under which diagenesis occurs.

- The ***early diagenetic realm*** (eogenesis or eogenetic zone, Fig. 2) occurs during burial to a few hundred meters and involves changes to the sediment, organic matter it hosts, and the interstitial fluids (pore water) by surface-related processes under near surface temperatures (≤30 °C). Diffusion of gases (e.g., oxygen, carbon dioxide, hydrogen sulfide, and methane) can also influence the geochemical environment. Early diagenesis typically involves dewatering of fine-grained sediments by gravitational compaction, bioturbation by burrowing organisms, dissolution of unstable minerals, diffusion of dissolved cations (e.g., Ca^{2+}, Mg^{2+}, Fe^{2+}, Mn^{2+}, Sr^{2+}), anionic species and gases (e.g., SO_4^{2-}, HCO_3^-, O_2, CO_2, CH_4, H_2S) through the sediment, bacterial decomposition of organic matter, transformation (neomorphism or recrystallization) of

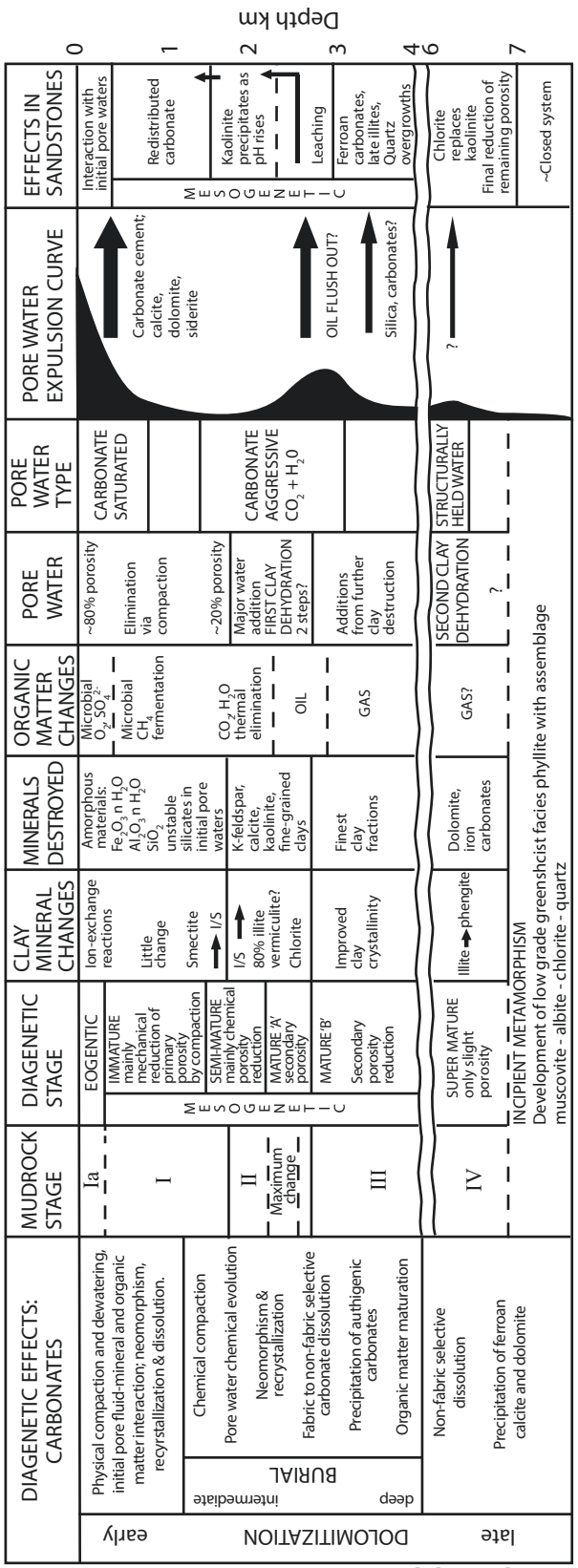

Diagenesis, Fig. 1 Matrix illustrating different aspects of diagenesis. The matrix is arranged with increasing depth (temperature) toward the bottom, and different sedimentary components in the columns (Modified from Burley et al. (1985))

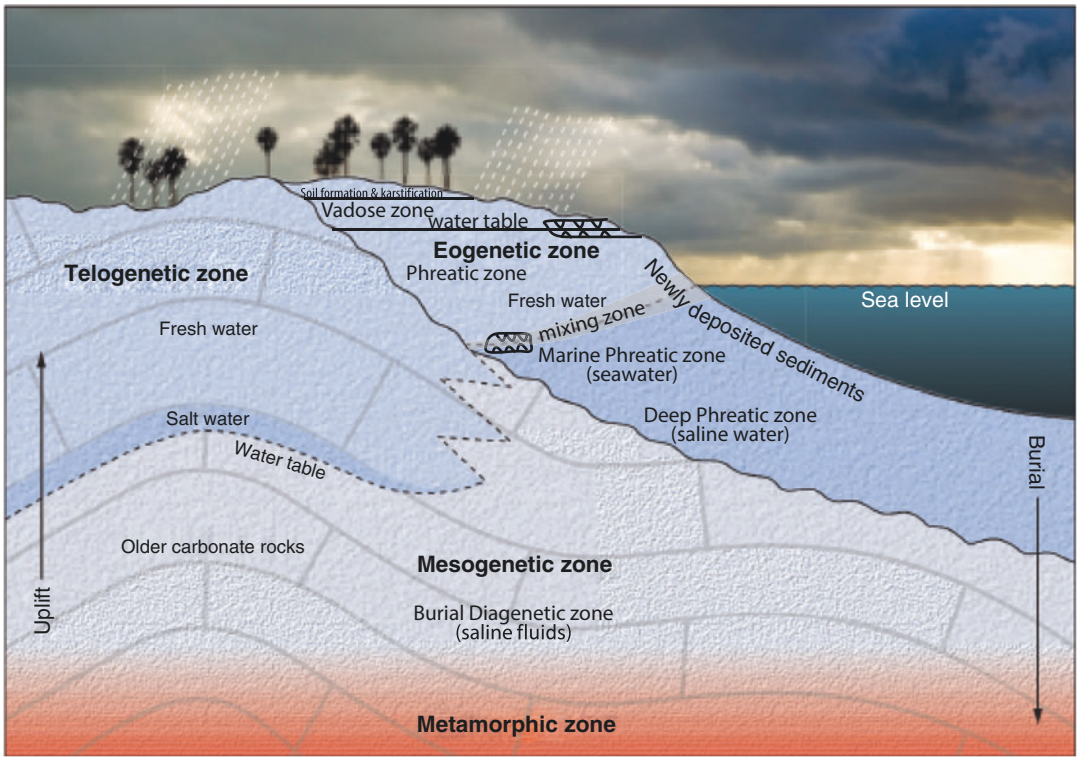

Diagenesis, Fig. 2 Summary of diagenetic realms. Sediments deposited in Earth surface environments pass through the diagenetic cycle post deposition, which can include the eogenetic zone (early diagenetic realm), the mesogenetic zone (burial diagenetic realm), and the telogenetic zone (exposure) (Modified from Ali et al. (2010))

unstable minerals, and precipitation of authigenic carbonates, oxides, hydroxy-oxides, aluminosilicates, sulfates, and sulfides. Sedimentation rate controls the degree of physical compaction and dewatering of sediments as well as the depths of bioturbation and cation/molecule diffusion rates. Most early diagenetic chemical reactions are driven by the reactivity of metastable minerals (e.g., amorphous silica, aragonite, high Mg-calcite, dolomite) or phyllosilicates. Many early diagenetic processes involve the kinetic boost by bacteria, referred to as bacterial mediation. Empirical studies of the early diagenetic realm involve outcrop studies and coring of marine and lake sediments and analysis of sediment mineralogy, texture, and grain size distribution, pore-water chemistry, and in recent years, the composition of associated microbial communities.

- Sediments continue to undergo geochemical modification in the ***burial diagenetic realm*** (mesogenesis or mesogenetic zone, Fig. 2) involving processes that are no longer directly related to the surface including chemical compaction (pressure solution), dissolution, precipitation of authigenic minerals (i.e., cementation), and organic matter maturation. This diagenetic realm is commonly partitioned into the intermediate burial (between 500 and 2000 m depth) and deep burial ($\geq$ 2 km) zones. Elevated temperature and pressure play a major role in driving the physicochemical reactions in the burial diagenetic realm. The chemical composition of pore waters evolves with depth, typically becoming more saline, due to fluid-rock interactions such as dewatering of clays and dissolution of buried evaporites. Maturation of organic matter releases organic acids and contributes toward lowering pH and changing redox conditions of interstitial fluids (Surdam and Crossey 1987; Harrison and Thyne 1992). Consequently, minerals, which were initially stable in the shallow diagenetic realm, become metastable with burial driving dissolution and precipitation of authigenic minerals such as calcite, dolomite, anhydrite, silica, zeolites, and clay mineral transformations. Overall, cementation is thought to dominate over dissolution in the burial diagenetic realm (Ali et al. 2010).
- Exposure of sedimentary rocks above base level by tectonic uplift (telogenesis) or sea-level fall exposes them to atmospheric processes and physical erosion and chemical weathering. Meteoric (fresh, dilute) waters can penetrate deeply into exposed or tectonically uplifted sedimentary rocks through permeable units or fracture porosity and develop extensive karst and dissolution features in carbonate-dominated successions (telogenetic zone, Fig. 2).

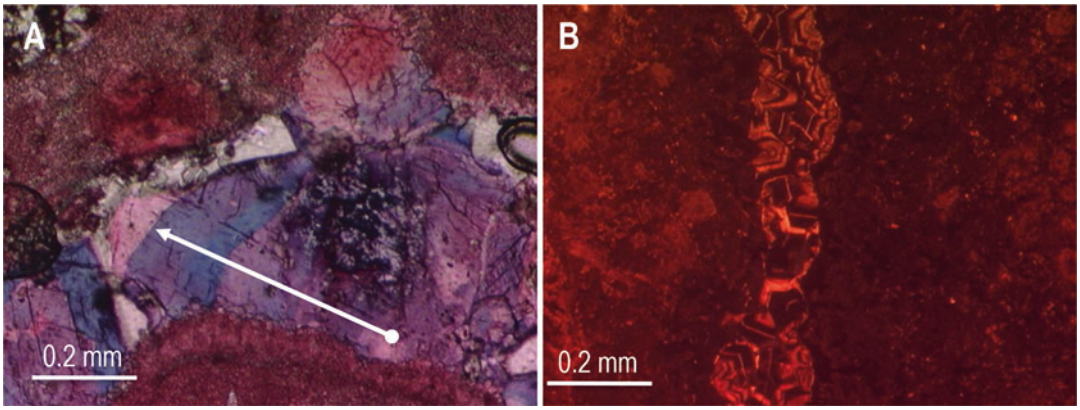

Diagenesis, Fig. 3 Photomicrographs of carbonate. (**a**) Stained (Alizarin *Red* and potassium ferricyanide) thin section showing calcite cement sequence (paragenesis) in a calcite spar cement that occludes a primary pore developed between grains (*pink*); thin marine cement and freshwater cement rims (*pink* staining are developed on grains. *White* triangular cement lining pores are dolomite. (**b**) Cathdoloumінescent zoning in calcite cement occluding porosity in a fracture (or between grains). The alternating bright luminescent and nonluminescent banding of the cement records the migration of multiple generations of calcite-precipitating fluids

- Tectonic forces and sea level fluctuations lead to cycling of sediments and sedimentary rocks between the diagenetic realms resulting in multiple cycles of dissolution, cementation, mineral transformation, and recystallization until a steady state or equilibrium is reached. The extent and nature of diagenesis will reflect the reactivity of the initial sediment, its fluid-rock interaction history including fluid-rock ratios and exposure time to each diagenetic zone.
- Where multiple diagenetic events have influenced a sedimentary rock, the paragenetic sequence of these events (Fig. 3) can be reconstructed by integrating microscope (thin sections to scanning electron microscopy) and geochemical studies of the sedimentary rocks and their fluid inclusion waters as well as associated organic matter. Diagenetic transformation of sedimentary rocks can substantially impact their porosity and permeability and in turn their fluid conduit and aquifer or reservoir potential (Montañez 1997).

Methods Applied to Study of Siliciclastic and Carbonate Rocks

Petrographic study of thin sections employing the optical microscope forms the basis for understanding the composition (mineralogy), spatial and textural relationships between detrital grains, authigenic minerals, and pore geometries (Fig. 3). Optical examination is aided by specialized preparation (impregnation of the rock with colored epoxy to highlight porosity) and staining techniques for recognition of specific carbonate minerals (Fig. 3a) and feldspars as well as calcite cements of differing Fe^{2+} concentration (Nelson and Read 1990; also see Humphries (1992) for a guide to thin section preparation methods). Cathodoluminescence study of thin sections (Fig. 3b) is commonly used to further identify textures and to define a paragenetic sequence for a given sample or suite of samples. A paragenesis is the sequence in which different minerals or generations of a given mineral (e.g., calcite) were precipitated. Carbonate cements exhibit varying shades of brown, red, yellow, and orange under cathodoluminescence due to incorporation of varying amounts of Fe^{2+} and Mn^{2+} into the crystal lattice. Cathodoluminescent zoning in carbonate cements reflects the Mn^{2+} to Fe^{2+} ratio of a given generation of carbonate cement, and in turn that of the fluid from which it precipitated. Authigenic feldspar overgrowths and cements are nonluminescent, whereas detrital cores and grains exhibit blue luminescence. Discrete generations of carbonate cements typically are identified by their coupled staining and cathodoluminescence (Fig. 3).

X-ray diffraction (XRD) is the preferred method for structural identification of fine-grained minerals, particularly in mudrocks. Moore and Reynolds (1989) provide a summary of preparation and analysis: Brindley and Brown (1984) and Newman (1987) provide detailed descriptions of clay minerals.

Geochemical analysis may include elemental and isotopic (both stable and radiogenic) approaches. While a comprehensive survey of all methods is beyond the scope of this overview, several common techniques will be mentioned. Electron microbeam techniques are powerful tools for in situ chemical and mineralogical examination of sedimentary rocks of all types. Scanning electron microscopy (SEM) is widely used to understand three-dimensional morphology, pore geometries, sequence of mineral growth, and more recently, microbe/mineral interactions (Banfield and Nealson 1997). Electron microprobe analysis (EMPA) provides quantitative chemical analyses of phases typically of 10 micron and greater size though specialized instruments may target smaller regions. This tool is generally restricted to major and minor element analysis. The secondary ion microprobe (SIMS) has gained

wide use in geoscience applications (see review in Stern 2009) and provides quantitative trace element and stable isotopic analyses in spatial context. Methods involving laser ablation in tandem with inductively coupled plasma mass spectrometry are providing new approaches to both elemental and isotopic analysis of sedimentary materials with excellent opportunities for application to diagenesis research (see examples in Rasbury et al. 2012). Integration of petrographic features with elemental and isotope analysis (carbon, oxygen, sulfur, and nitrogen) of authigenic phases, at times coupled with fluid inclusion study, has been effective in understanding conditions of formation and paleofluid composition in some cases (see summaries in Sharp 2007). Banner (2004) provides a comprehensive overview of applications of radiogenic isotopes to sedimentary systems.

Carbonate Diagenesis

Carbonates are minerals with a structural CO_3^{2-} group and Ca^{2+}, Mg^{2+}, or a combination of these two elements. Weight percent Fe^{2+}, Mn^{2+}, and Sr^{2+} occur in less common carbonates. Most carbonate sediments form in marine settings commonly with coexisting polymorphs of aragonite and low- ($\leq$5% $MgCO_3$) to high-Mg calcite (5–20% $MgCO_3$), as well as rarely dolomite (Moore 1989). Terrestrial carbonates form as low-Mg calcite and siderite in lacustrine, wetland, and spring deposits, low-Mg calcite and sphaerosiderites in soils, and low- to high-Mg calcite and aragonite in travertines and cave speleothems. This entry focuses on marine carbonates given their prevalence in the modern and geologic record; see reviews by Ford and Pedley (1996) and Capezzuoli et al. (2014) for freshwater carbonates.

Carbonate mineralogy in the marine realm is determined thermodynamically by mineral stability (solubility) and kinetically by substrate mineralogy, biological effects, differences in precipitation rates, and the presence/absence of organic compounds and inorganic inhibitors (e.g., SO_4^{2-}, PO_4^{3-}, Mg^{2+}) (Burton 1993). Biological effects include microbial mediation and vital effects. With the exception of low-Mg calcite, all of these carbonate mineralogies are thermodynamically metastable (high Mg-calcite, aragonite, non-stoichiometric dolomite) at Earth surface conditions and will convert to stable low-Mg calcite or stoichiometric dolomite during subsequent exposure to evolved marine pore waters, introduction of meteoric fluids, and/or interaction with saline brines during burial (Walter 1985).

Early Diagenetic Realm

For shallow-water carbonates, extensive diagenesis occurs proximal to the sediment-fluid or atmosphere interface due to repeated flushing by seawater or freshwater (eogenetic zone, Fig. 2). Their metastable mineralogy makes them highly susceptible to post-depositional mineralogical and geochemical alteration as the pore fluid chemistry evolves with fluid mixing and chemical reactions (Moore 1989; James and Choquette 1990). Diagenesis at the sediment-seawater interface begins with boring by endolithic algae, sponges, and fungi, which replace primary skeletal carbonate with clay-size carbonate precipitates (micrite), a process called micritization. Within the first few centimeters to meters of burial, dissolution of high-Mg calcite and aragonite releases bicarbonate (HCO_3^-) that along with fluid CO_2 degassing promotes neomorphism and recrystallization of grains, carbonate cementation, and calcite overgrowths on biotic templates. Neomorphism involves the molecular-scale replacement of an unstable phase of carbonate by thermodynamically more stable low-Mg calcite. Recrystallization of grains and early cements involves the wholesale dissolution of the original carbonate and simultaneous precipitation of a more stable phase resulting in a possible volume change and loss of original textures. Recrystallization occurs in both carbonates and siliciclastic deposits. These early diagenetic processes lead to preservation of much of the original fabric and retard compaction in shallow-water marine carbonates. Dissolution of aragonitic fossils and matrix creates secondary moldic or vuggy porosity.

In contrast to shallow-water carbonates, the predominance in deep-sea sediments of stable low-Mg calcite causes delay in dissolution and cementation. The presence of small amounts of calcite overgrowths and cements on shells and shell recrystallization indicates localized regions of carbonate dissolution and diffusion/advection to areas of calcite cementation (Moore 1989). Oxidation of organic matter buried with carbonate sediments provides HCO_3^- to pore fluids for carbonate precipitation. Pore water profiles of the oxygen ($\delta^{18}O$) and calcium ($\delta^{44}Ca$) isotopic composition and trace element concentrations are used to model the rates of carbonate recrystallization in deep-sea sediments (Fantle et al. 2010). Gravitational compaction of deep-sea sediments in the shallow burial realm (within the first 200 m of burial) is a major influence on lithification and leads to substantial loss of porosity (from ~80% to $\leq$50–60%).

The diagenetic evolution of carbonate sediments, which were deposited on the slopes surrounding shallow-water carbonate platforms, falls between that of deep-sea sediments and shallow-water marine carbonates. This reflects the mixing of a pelagic low-Mg calcite source with a platform-shed source of reactive aragonite and high-Mg calcite as well as overall higher concentrations of organic matter (Swart 2015). Thus, periplatform carbonates may undergo extensive dissolution and cementation during initial burial making them more resistant to compaction than deep-sea sediments.

Meteoric diagenesis: The vast majority of carbonates are deposited during sea level highstands when shallow water platforms are inundated (Ali et al. 2010). These carbonates

are subsequently exposed to freshwater, which is undersaturated with respect to carbonates, during subsequent drop in base level whether driven by eustasy or tectonic uplift (telo- or epidiagenesis). Meteoric diagenesis occurs over a series of near-surface (eogenetic) diagenetic zones (Fig. 2) including soil formation and karstification and vadose, phreatic, and mixing zones (see reviews by Moore 1989; James and Choquette 1990). Overall, freshwater reactions with metastable carbonates result in extensive stabilization (through neomorphism or recrystallization) of carbonate grains, superimposed generations of dissolution and low-Mg calcite cementation, as well as substantial redistribution of pore space. The degree of diagenetic alteration is dictated by the reactivity of the initial mineralogy, the pore fluid chemistry, fluid-rock ratios, and flow rates.

Diagenesis in the freshwater undersaturated vadose zone is characterized by seepage flow through intergranular porosity and conduit flow through solution-enlarged fissures (Fig. 2). Vadose waters are typically CO_2-charged and chemically aggressive given exchange with the atmosphere and with soil-formed CO_2. Rapid conduit flow leads to extensive, non-mineral selective dissolution. Rates of calcite precipitation are far slower than fluid flow rates, thus as dissolution proceeds fluids become oversaturated with respect to low-Mg calcite and precipitate cements down-flow (Moore 1989). Freshwater that percolates slowly through the vadose zone by diffuse flow promotes mineral-controlled diagenesis, which is controlled by the differing solubilities of the carbonate polymorphs. Aragonite is 1.5 times more soluble than low-Mg calcite at a given temperature, whereas high-Mg calcite, whose solubility increases with Mg content, can be up to an order of magnitude more soluble than low-Mg calcite (Walter 1985). Dissolution of more soluble carbonate under the slow diffuse flow rates leads to oversaturation with respect to low-Mg calcite proximal to the site of dissolution driving widespread fabric-retentive neomorphism, recrystallization, and precipitation of vadose calcite cements (e.g., pendant and meniscus cements, crystal silt, fine crystalline equant cements unevenly lining primary porosity). The end-product can be wholesale transformation of metastable carbonates to thermodynamically stable low-Mg calcite while retaining much primary texture and fabric. This conversion process, however, is slow (on the order of 10^6 year) reflecting the overall low water-rock ratios of the vadose zone.

The water table (Fig. 2) delineates the boundary between the vadose and underlying saturated phreatic zone. High flow rates and turbulent exchange at the water table promotes CO_2 dissolution into water or high CO_2 degassing rates making this region a dynamic zone of dissolution and low-Mg cementation (Moore 1989; James and Choquette 1990). The phreatic zone hosts the bulk of dissolution and cementation by freshwater. Exposure of marine carbonates due to sea level fall leads to deep penetration of meteoric water given that the freshwater phreatic lens will develop to depths of ~40 times the height of the water table above sea level (Ghyben–Herzberg principle). Diagenetic processes in the shallow phreatic zone are orders of magnitude faster than in the vadose zone reflecting overall higher flow rates and fluid-rock ratios. In this zone, low-Mg calcite cements form isopachous rims of equant to bladed crystals on grains and within moldic porosity and microspar cements partially to fully occlude porosity. Relatively rapid flow rates lead to large-scale transport of dissolved carbonate and Ca^{2+} down-flow resulting in extensive dissolution updip and cementation downdip.

Mineralogic stabilization within the phreatic zone (Fig. 2) occurs rapidly (10^4–10^5 year) relative to the vadose zone. Once stabilized, subsequent diagenetic modification is limited to minor cementation within conduits that focus fluid flow. The mixing zone (Fig. 2), at the interface between the freshwater phreatic zone and the underlying deep phreatic zone with saline continental or marine interstitial fluids, is a chemically active region given that physical and diffusive mixing of waters leads to nonlinear changes in carbonate mineral saturation. The mixing zone is a region of abundant secondary porosity and subsurface karst development (e.g., Boulder zone in the Tertiary Florida aquifer or the ceynotes of the Yucatan Peninsula). The different zones of meteoric diagenesis have characteristic stable (O and C) isotopic and trace element signatures that when coupled with stratigraphic and petrographic studies have been used to reconstruct the diagenetic history of carbonate successions. The reader is directed to Moore (1989) and Swart (2015) for a comprehensive review of the geochemistry of meteoric diagenesis. The deep phreatic zone (Fig. 2) is a shallow burial locale of substantially slower diagenesis given the slow fluid flow rates and low fluid-rock ratios. Low-Mg calcite and dolomite cements that form in this zone are typically large and blocky reflecting their slow growth rates under very low saturation states.

The meteoric diagenetic realm is dynamic with fluctuations in base level, whether driven by eustasy or tectonics, that induce repeated large-scale vertical migration of the marine, vadose, phreatic, and mixing zones through a sedimentary succession over time (Read and Horbury 1993). Throughout Earth history, sea level has fluctuated 10 s to 100 s of m over a spectrum of timescales (10^4–10^7 -year) driven by orbitally forced waxing and waning of ice sheets, atmospheric pCO_2 variability, and tectonic and mantle processes. These shifts in the meteoric diagenetic zones impart a mineralogic and geochemical signature that is characteristic of the magnitude of relative sea-level fluctuations and the climate regime under which they occurred (Read and Horbury 1993). Zonation in low-Mg calcite cements, discernible petrographically under transmitted light or by cathodoluminescence (Fig. 3) as well as by their geochemical compositions (Fe, Mn, Mg,

concentrations and $\delta^{18}O$ and $\delta^{13}C$ isotopic compositions), record changes in fluid conditions (redox, temperature, salinity) through time from which the spatial migration of the near-surface diagenetic zones can be reconstructed (Niemann and Read 1988; Nelson and Read 1990). In many cases, zoned phreatic cements capture multiple cycles of fluid change within a pore providing a strip chart of the eustatic fluctuations that affected a given carbonate succession (Read and Horbury 1993) even when deeply eroded by post-depositional processes (Bishop et al. 2009).

Intermediate-to-Deep Burial Diagenetic Realm

Ultimately, most sedimentary deposits are buried sufficiently (>1 km) by overlying sediments and rocks that they are introduced to the intermediate-to-deep-burial diagenetic realm (herein referred to as "burial diagenetic" or mesogenetic zone). The burial diagenetic zone (Fig. 2) begins proximal to the liquid oil window in hydrocarbon source rocks (Machel 2005). Formation temperatures are elevated above ~50 °C reaching conditions of over 100–200 °C, which enhances diagenetic reactions. The burial diagenetic realm is characterized by further chemical compaction and dissolution, mineral stabilization, and precipitation of cements. Depending on the clay mineral content and previous cementation history, chemical compaction can become a predominant process with the degree of pressure solution influenced by pore-water composition, mineralogy, degree of previous cementation, and the presence of organic matter. Grains or primary marine cements or earlier diagenetic precipitates, which were not previously stabilized, become thermodynamically metastable in the deep subsurface due to changing fluid conditions driving further recystallization and mineral replacement, including widespread dolomite replacement of limestone host rocks (Machel 2005).

Interstitial (formation) fluids in the deep-burial diagenetic environment range from brackish (< 35 weight percent) to hypersaline reflecting their interaction history with sedimentary rocks, including evaporites and siliciclastics, along their flow path and mixing with organic-rich fluids, which formed during hydrocarbon maturation. Fluid flow rates vary from near stagnant to moderately fast if an external hydraulic gradient is established by regional groundwater flow systems or dewatering of shale basins. At temperatures proximal to and within the oil window (~80–120 °C), thermal maturation of organic matter (decarboxylation) and other mineral reactions occurring in situ or in shale basins introduce organic-acid, CO_2-rich brines that can lead to extensive non-fabric-specific dissolution (Montañez 1994, 1997; Machel 2005). As these fluids evolve down-flow through wholesale dissolution and pressure solution, they become saturated and precipitate Fe- and Mg-rich calcite cements and Ca-rich dolomites (Montañez 1994). Dolomite, anhydrite, and silica (chert) replacement of limestones is common in the deep-burial diagenetic realm. Exposure of evaporite-rich deposits to hydrocarbon-bearing fluids at elevated temperatures promotes thermochemical sulfate reduction, which produces significant amounts of H_2S and water and precipitation of low-Mg calcite and pyrite, and possibly saddle dolomite (Swart 2015). At temperatures <80–100 °C, bacterial sulfate reduction dominates when dissolved sulfate is exposed to hydrocarbons.

Ultimately, tectonic processes may uplift deeply buried carbonate successions and expose them to meteoric conditions. For those carbonates, which were previously stabilized and lithified in near-surface to deep-burial diagenetic zones, the extent of dissolution and cementation in this telogenetic zone (Fig. 2) will be greatly reduced. Rather, diagenesis will occur as karstification and development of fluid conduits associated with fractures and joints.

Dolomitization

The origin of dolomite, particularly early diagenetic dolomite, remains elusive despite over a century of empirical and experimental studies. This reflects that dolomite ($CaMg(CO_3)_2$) is rare in modern environments but very common in ancient carbonate successions. Furthermore, constraints on the chemical and hydrologic conditions of dolomite formation are limited and the kinetics of dolomite precipitation are poorly understood (Machel 2004). Although seawater is ~1000 times oversaturated with respect to dolomite, it rarely forms in the marine realm given the need for a source and mechanism of steady Mg^{2+} supply (Swart 2015) and mechanism to overcome kinetic inhibitors (e.g., SO_4^{2-}). Thus, dolomite precipitation (i.e., primary dolomite) and replacement of $CaCO_3$ (i.e., dolomitization) at earth surface conditions require a mechanism to raise the saturation state of dolomite and provide the necessary high fluid-rock ratios for steady Mg^{2+} supply. Highly evaporative environments (arid climate tidal flats) and refluxing of evaporatively sourced brines through shallow-water carbonates (Montañez and Read 1992a), possibly in mafic parent-material or seasonally very dry soils (Capo et al. 2000) and fluids in which the alkalinity is increased by oxidation of organic matter provide such a mechanism for "early" dolomitization (Fig. 1; Machel 2004; Swart 2015). The fluid mixing zone at the interface between the freshwater phreatic lens and underlying deep phreatic zone has been invoked as a locale of dolomite formation (Fig. 2) given that fluid mixing leads to undersaturation with respect to calcite but high supersaturation with respect to dolomite. Dolomite, however, is absent from most modern-day mixing zones and ancient examples have been contested (Machel 2004; Swart 2015). Bacterial mediation is likely involved in the precipitation of many near surface dolomites (Vasconcelos et al. 1995), in particular in highly evaporative environments and/or organic-rich deposits. Early formed dolomites are typically poorly ordered and Ca-rich

(non-stoichiometric) and volumetrically minimal. These disordered and Ca-rich dolomites undergo stepwise recrystallization throughout burial, becoming more ordered and stoichiometric with time and with exposure to dolomitizing fluids (Montañez and Read 1992b). Progressive recrystallization overprints their original geochemical signature although a memory of the primary composition can be preserved.

Extensive dolomitization, however, likely occurs in the intermediate- (100 s m) to deep-burial realm (up to 1000s of m) (Fig. 1). This reflects the elevated temperatures needed to overcome kinetic inhibitors, the very high fluid-rock ratios, the hydrologic plumbing to provide the Mg^{2+} and CO_3^{2-} supply, and the time required to produce volumetrically large (massive) dolomites (Machel 2004). Normal seawater may be capable of extensive dolomitization at slightly elevated temperatures (50–80 °C) and moderate depths (few 100 meters) in regions of large-scale thermal circulation through isolated carbonate platforms (Kohout convection). Regional or basinwide dolomitization, however, likely develops through multiple generations of dolomite replacement of limestones and precipitation of dolomite cements (Montañez 1992, 1994). Hydrologic models invoked for regional dolomitization, in addition to thermal convection, include tectonically induced flow of basinal brines, funneled compaction flow, and rapid upward advection of hydrothermal fluids along faults (summarized in Machel 2004), although the latter process is likely limited in spatial scope. Integration of stratigraphy, petrographic (textures and cathodoluminescent zoning) features, and geochemical compositions of dolomite and its fluid inclusion waters has been effectively used to unravel the paragenesis of multigeneration massive dolomites (e.g., Montañez 1994) and to reconstruct the hydrology of dolomitizing environments (studies summarized in Machel 2004; Swart 2015; and Montañez 1992, 1994). Massive dolomites (dolostones) in the subsurface tend to have higher porosities than limestones making them excellent reservoirs (Montañez 1997). Enhanced porosity is attributed to (1) a 12% porosity increase during replacement given the smaller molar volume of dolomite relative to calcite, (2) dissolution of original calcite during burial dolomitization or during subsequent migration of low pH brines, and/or (3) thermochemical sulfate reduction.

Siliciclastic (Sandstones and Mudrock) Diagenesis

The diagenesis of siliciclastic grains encompasses the full range of grain sizes found in sedimentary systems. Siliciclastic systems usually are composed of a primary population of detrital grains and primary porosity. A summary of the controls on initial composition of clastic grains may be found in Johnsson (1993). Common physical diagenetic changes in siliciclastic sediments include compaction, bioturbation, and tectonic deformation. All three of these processes may result in the rearrangement of primary grains, hence influence the porosity and permeability of the unconsolidated sediment. Compaction acts to reduce primary porosity, and may reduce both inter- and intragranular volume. Deformation may result in crushing of primary grains as well as cross-cutting fractures in lithified rocks. Chemical diagenetic changes in siliciclastic systems involve fluid-rock interaction and result in mineral precipitation, dissolution, or recrystallization. Examples include recrystallization of metastable or unstable phases, precipitation of new, authigenic phases as grain replacement or intergranular cement, and dissolution of unstable phases resulting in secondary porosity. While many cements and mineral reactions appear to result from predictable, equilibrium processes, it is common for siliciclastic sediments and rocks to be in an overall state of chemical disequilibrium due to the presence of a wide range of primary constituents and the relatively low temperatures (hence slow reaction rates) particularly during early diagenesis. Figure 1 highlights some important depth-related changes in clastic rocks. Original grain composition, increasing temperature and pressure, the hydrodynamic conditions, and the presence of reactive organic matter all play an important role in determining the extent of diagenetic modification.

Early Diagenesis

During early diagenesis, the precipitation of carbonate minerals (especially, calcite, ankerite, and siderite), quartz, and aluminosilicates such as kaolinite, smectite and illite predominate. If oxidizing conditions are encountered (as through active meteoric recharge in the near-surface (eogenetic) environment), oxides and hydroxides of iron and manganese may form as well (these include ferrihydrite, goethite, limonite, todorokite, and pyrolusite). High water throughput or excess acidity during early diagenesis may also result in selective dissolution of primary grains (especially carbonates) or alteration of lithic and feldspar grains to produce secondary porosity in addition to authigenic clays. Some primary clastic assemblages, for example, volcanic materials including glass, result in high pH conditions that foster the formation of zeolites in addition to clay minerals. An extensive theoretical treatment of early diagenesis is provided in Berner (1980).

Burial Diagenesis

During burial, shales undergo dewatering including compaction-driven expulsion and loss of water from dehydration of silicates (clay minerals). In sandstones, authigenic growth of quartz (commonly as syntaxial overgrowths on existing clean quartz grain surfaces), kaolinite (often accompanying detrital feldspar alteration), smectite, illite, and calcite dominates. At greater depths, mixed-layer clays become

more illitic and chlorite, dolomite, and ankerite are more common. Detrital feldspars alter toward more sodic compositions (albitization). The geochemistry of authigenic phases, as well as of fluid inclusions within these minerals, provides information on the burial conditions.

Novel Approaches to Studying Diagenesis

The study of carbonate diagenesis is experiencing a rejuvenation with the introduction of new visualization, geochemical proxy and modeling approaches. Although petrographic and SEM study coupled with geochemical analysis of carbonate and siliciclastic rocks have become fundamental tools for reconstructing diagenetic pathways and environments, a new suite of stable (boron, sulfur, magnesium, calcium, lithium) and radiogenic (Sr, Nd, U) isotopes are being applied to carbonates to reconstruct paleo-seawater pH, oxygenation, and temperature as well as to place constraints on past carbon, sulfur, and magnesium cycling, weathering rates, and crystallization rates. Such studies have implications for the evolution of pCO_2 and pO_2 and life-environment interactions. With the advent of better methods for determination of trace element concentrations and their isotopic compositions through applications of ICP-MS, the use of trace metals as paleo-redox and paleoproductivity proxies has led to a rich literature (Lyons et al. 2014; Tribovillard et al. 2006; Gill et al. 2011; Jones and Manning 1994). Of particular interest for diagenetic studies is clumped isotope paleothermometry (Δ_{47}), which uniquely permits independent measurements of carbonate cement precipitation temperatures in carbonate and siliciclastic sedimentary rocks and the $\delta^{18}O_{fluid}$ in which they formed. Although the application of clumped isotope thermometry to diagenetic studies is only beginning, initial results show promise for constraining diagenetic conditions and the evolution of fluid-flow conduits (Huntington et al. 2011; Budd et al. 2013). These applications of sedimentary geochemistry require assessment of separate diagenetic effects from primary signals in rocks across the broadest range of time scales. A surge in computational power over the past two decades is permitting the integration of sedimentology, petrography, geochemistry, geodynamics, and structural geology into forward modeling of the diagenetic evolution of sedimentary successions and the impact of diagenesis on their petrophysical properties and hydrologic potential (e.g., Whitaker et al. 2014; Agar and Geiger 2015).

Summary

Diagenetic modification of freshwater and marine carbonates and siliciclastic deposits by physical and chemical processes is a dynamic process that begins immediately following deposition (0–30 °C) through to the metamorphic realm (~250 °C). Sediments are converted to sedimentary rocks, and permeability and porosity develop by the integrated effects of dissolution, cementation, mineral overgrowth, neomophism, and recrystallization. The extent of diagenetic modification is governed by the original grain composition and reactivity, temperature and pressure, hydrodynamic conditions, and the presence of reactive organic matter. Bacterial mediation is an important component of carbonate and siliciclastic diagenesis.

The diagenetic cycle includes the early (eogenetic) through burial (mesogenetic) diagenetic realms as well as the telogenetic zone associated with tectonic uplift or sea-level exposure of sedimentary rocks. Although dolomite has been shown to form at Earth's surface conditions with microbial mediation, extensive dolomitization occurs in the burial realm where kinetic inhibitors are overcome and elevated temperatures and high fluid-rock ratios promote the process. Maturation of sedimentary hosted organic matter through the diagenetic cycle has produced the world's coal, oil, and gas deposits. Modern diagenetic studies are coupling new visualization, geochemical proxy, and modeling approaches with fundamental petrographic and geochemical tools in order to (1) quantitatively constrain the diagenetic history of carbonate and siliciclastic successions, (2) assess the potential of sedimentary rocks as archives of past surface conditions, and (3) reconstruct the evolution of petrophysical properties and hydrologic conduits in sedimentary units, as well as their resource potential.

Cross-References

► Fluid–Rock Interaction

References

Agar SM, Geiger S (2015) Fundamental controls on fluid flow in carbonates: current workflows to emerging technologies. In: Agar SM, Geige S (eds) Fundamental controls on fluid flow in carbonates: current workflows to emerging technologies. Geological Society of London, London, UK, no. 406. pp 1–59

Ali SA, Clark WJ, Moore WR, Dribus JR (2010) Diagenesis and reservoir quality. Oilfield Rev 22(Summer Issue):1–27

Banfield JF, Nealson KH (eds) (1997) Geomicrobiology: interactions between microbes and minerals. Reviews in mineralogy, 35. The Mineralogical Society of America, Washington, DC, 448 p

Banner JL (2004) Radiogenic isotopes: systematics and applications to earth surface processes and chemical stratigraphy. Earth Sci Rev 65:141–194

Berner RA (1980) Early diagenesis: a theoretical approach, vol 1. Princeton University Press, Princeton

Bishop JW, Montañez IP, Gulbranson EL, Brenckle PL (2009) The onset of mid-Carboniferous glacio-eustasy: sedimentologic and diagenetic constraints, Arrow Canyon, NV. Palaeogeogr Palaeoclimatol Palaeoecol 276:217–243

Brindley G, Brown G (1984) Chrystal structures of clay minerals and their X-ray identification. Mineral Soc Monogr 5:504 p
Budd DA, Frost EL III, Huntington KW, Allwardt PF (2013) Syndepositional deformation features in high-relief carbonate platforms: long-lived conduits for diagenetic fluids. J Sediment Res 83:14–38
Burley S, Kantorowicz JD, Waugh B (1985) Clastic diagenesis. Sedimentology 18:189–226
Burton EA (1993) Controls on marine carbonate cement mineralogy: review and reassessment. Chem Geol 105:163–179
Capezzuoli E, Gandin A, Pedley M (2014) Decoding tufa and travertine (fresh water carbonates) in the sedimentary record: the state of the art. Sedimentology 61:1–21
Capo RC, Whipkey CE, Blachere JR, Chadwick O (2000) Pedogenic origin of dolomite in a basaltic weathering profile, Kohala Peninsula, Hawaii. Geology 28:271–274
Choquette PW, Pray LC (1970) Geologic nomenclature and classification of porosity in sedimentary carbonates. Bull Am Assoc Pet Geol 54:207–250
de Segonzac DG (1968) The birth and development of the concept of diagenesis (1866–1966). Earth Sci Rev 4:153–201
Fairbridge RW (1967) Phases of diagenesis and authigenesis. In: Larsen G, Chilinger GV (eds) Diagenesis in sediments. Elsevier, Amsterdam, pp 19–89
Fantle MS, Maher KM, DePaolo DJ (2010) Isotopic approaches for quantifying the rates of marine burial diagenesis. Rev Geophys 48:1–48
Ford ND, Pedley HM (1996) A review of tufa and travertine deposits of the world. Earth Sci Rev 41:117–175
Gill BC, Lyons TW, Young SA, Kump LR, Knoll AH, Saltzman MR (2011) Geochemical evidence for widespread euxinia in the later Cambrian ocean. Nature 469:80–83
Harrison W, Thyne G (1992) Predictions of diagenetic reactions in the presence of organic acids. Geochim Cosmochim Acta 56:565–586
Humphries DW (1992) The preparation of thin sections of rocks, minerals, and ceramics. Oxford University Press, Oxford, 83 p
Huntington KW, Budd DA, Wernicke BP, Eiler JM (2011) Use of clumped-isotope thermometry to constrain the crystallization temperature of diagenetic calcite. J Sediment Res 81:656–669
James NP, Choquette PW (1990) Limestones – the meteoric diagenetic environment. In: McIlreath IA, Morrow DA (eds) Diagenesis reprint series 4. Geoscience Canada, Geological Association of Canada, St. John's, NL A1B 3X5 Canada, pp 35–73
Johnsson MJ (1993) The system controlling the composition of clastic sediments. Geol Soc Am Spec Pap 284:1–20
Jones B, Manning DA (1994) Comparison of geochemical indices used for the interpretation of palaeoredox conditions in ancient mudstones. Chem Geol 111:111–129
Larsen G, Chilingar GV (eds) (1983) Diagenesis in sediments and sedimentary rocks, 2. Developments in sedimentology 25B. Elsevier, Amsterdam, 563 p
Lyons TW, Reinhard CT, Planavsky NJ (2014) The rise of oxygen in earth's early ocean and atmosphere. Nature 506:307–315
Machel HG (2004) Concepts and models of dolomitization: a critical reappraisal. In: Braithwaite CJR, Rizzi G, Darke G (eds) The geometry and petrogenesis of dolomite reservoirs. Geological Society of London, London, no. 235. pp 7–63
Machel HG (2005) Investigations of burial diagenesis in carbonate hydrocarbon reservoir rocks. Geosci Can 32:103–128
Montañez IP (1992) Controls of eustasy and associated diagenesis on reservoir heterogeneity in Lower ordovician, upper knox carbonates, appalachians. In: Candelaria MP, Reed CA (eds) Paleokarst, karst related diagenesis, and reservoir development: examples from ordovician-devonian age Strata of West Texas and the Mid-Continent, Permian basin section SEPM special publication, SEPM (Society for Sedimentary Geology), Tulsa, OK no. 92-33. pp 165–181
Montañez IP (1994) Late diagenetic dolomitization of Lower Ordovician Upper Knox Carbonates: a record of the hydrodynamic evolution of the southern Appalachian Basin. Am Assoc Pet Geol Bull 78:1210–1239
Montañez IP (1997) Secondary porosity and late diagenetic cements of the Upper Knox Group, central Tennessee region: a temporal and spatial history of fluid flow conduit development within the Knox regional aquifer. In: Montañez IP, Gregg JM, Shelton K (eds) Basinwide fluid flow and associated diagenetic patterns: integrated petrologic, geochemical and hydrologic considerations, SEPM special publication, no. 57. pp 101–117
Montañez IP, Read JF (1992a) Eustatic control on early dolomitization of cyclic peritidal carbonates: evidence from the early ordovician upper knox group. Appalachians Geol Soc Amer Bull 104:872–886
Montañez IP, Read JF (1992b) Fluid-rock interaction history during stabilization of early dolomites of the upper knox group (early ordovician). Appalachians J Sediment Petrol 62:753–778
Moore CH (1989) Carbonate diagenesis; porosity evolution and diagenesis in a sequence stratigraphic framework, Developments in sedimentology, vol 46. Elsevier, Amsterdam, 321 p
Moore DM, Reynolds RC (1989) X-ray diffraction and the identification and analysis of clay minerals 378. Oxford University Press, Oxford
Nelson WA, Read JF (1990) Updip to downdip cementation and dolomitization patterns in a Mississippian aquifer. Appalachians J Sediment Petrol 60:379–396
Newman ACD (1987) Chemistry of clays and clay minerals, Mineralogical society monograph, vol 6. Wiley, New York, 480 p
Niemann JC, Read JF (1988) Regional cementation from unconformity-recharged aquifer and burial fluids, Mississippian Newman Limestone, Kentucky. J Sediment Petrol 58:688–705
Rasbury ET, Hemming S, Riggs N (2012) Mineralogical and geochemical approaches to provenance. Geological Society of America special paper 487
Read JF, Horbury AD (1993) Eustatic and tectonic controls on porosity evolution beneath sequence-bounding unconformities and parasequence disconformities on carbonate platforms. In: Horbury AD, Robinson AG (eds) Diagenesis and basin development: studies in geology, vol #36. American Association of Petroleum Geologists, Tulsa, pp 155–197
Sharp Z (2007) Principles of stable isotope geochemistry. Pearson Education, Upper Saddle River, 344 p
Stern RA (2009) Introduction to secondary ion mass spectrometry (SIMS) in geology. In: Fayek M (ed) Secondary ion mass spectrometry in the earth sciences, Mineral. Association of Canada, Short Course Series, 41, pp 1–18
Surdam RC, Crossey LC (1987) Integrated diagenetic modeling: a process-oriented approach for clastic systems. Annual Rev Earth Planet Sci 15:141–170
Surdam RC, Crossey LJ, Hagen ES, Heasler HP (1989) Organic-inorganic interactions and sandstone diagenesis. Amer Assoc Petrol Geol Bull 73:1–23
Swart PK (2015) The geochemistry of carbonate diagenesis: the past, present and future. Sedimentology 62:1233–1304
Tribovillard N, Algeo TJ, Lyons T, Riboulleau A (2006) Trace metals as paleoredox and paleoproductivity proxies: an update. Chem Geol 232:12–32
Vasconcelos C, McKenzie JA, Bernasconi S, Grujic D, Tien AJ (1995) Microbial mediation as a possible mechanism for natural dolomite formation at low temperatures. Nature 377:220–222
Walter LM (1985) Relative reactivity of skeletal carbonates during dissolution: implications for diagenesis. In: Schneidermann N, Harris PM (eds) Carbonate cements. SEPM special publication, no. 36. Tulsa, pp 3–16
Whitaker FF, Felce GP, Benson GS, Amour F, Mutti M, Smart PL (2014) Simulating flow through forward sediment model stratigraphies: insights into climatic control of reservoir quality in isolated carbonate platforms. Pet Geosci 20:27–40

Diffusion

Yan Liang
Department of Earth, Environmental and Planetary Sciences, Brown University, Providence, RI, USA

Definition

Diffusion arises from random motions of particles in a fluid or solid. Here the particles can be neutral molecules or atoms, or charged cations or anions. The particle that diffuses through a medium or substance is called diffusant. Diffusion is a microscopic kinetic phenomenon that results in intermingling and homogenization of the chemical components in a substance. It is part of the mixing process that is not accounted for by the bulk flow or advection of the chemical system. The word "diffusion" originates from the Latin word "diffundere" which means to pour out or spread out.

Fick's Laws of Diffusion

The spreading of diffusant in a medium can be quantified by applying the laws of diffusion which are established through observations of natural phenomenon and laboratory diffusion experiments. During diffusion, random motions of the particles in a chemically heterogeneous phase will redistribute its constituent from regions of high concentration to low concentration, which eventually leads to homogenization of the phase. The amount of materials that move perpendicular through a unit cross-section area by diffusion or random motions of the particles in the medium is called diffusive flux. According to Fick's first law of diffusion, the diffusive flux for a component of interest, $\mathbf{J_i}$, is proportional to the concentration gradient of the component in the system. For one-dimensional diffusion, this can be written as

$$\mathbf{J_i} = -D_i \frac{\partial c_i}{\partial x}, \tag{1}$$

where D_i is the diffusion coefficient or diffusivity of component i; c_i is the concentration of component i; and $\partial c_i/\partial x$ is the concentration gradient of component i along the x direction. The diffusive flux has the units of mass per unit area per unit time. The concentration has the units of mass per unit volume. The diffusion coefficient has the units of length-squared per unit time, for example, $m^2\ s^{-1}$. The diffusive flux is a vector (along x direction in this case) and the negative sign in Eq. 1 is to ensure that material diffuses from regions of high concentration to low concentration, that is, along the direction of decreasing concentration gradient.

Fick's first law of diffusion was postulated by Adolf Fick in 1855, drawing on the analogy between the spreading of a solute in a solvent to Fourier's law for the diffusion of heat by conduction and Ohm's law for the flow of electric current in a conductor (Tyrrell 1964; Narasimhan 2004). It was based on observations of diffusion in a binary solution (salt and water in Fick's case). The term interdiffusion has also been used to describe diffusion in a binary liquid or solid (e.g., diffusion of salt in water or Fe-Mg diffusion in olivine). The diffusion coefficient obtained from a binary diffusion experiment is called the interdiffusion coefficient. Fick's first law has been used to define the diffusion coefficient and to study steady-state diffusion along a concentration gradient.

Fick's second law of diffusion is a statement of mass conservation for diffusive mass transfer in a medium. In one dimension, the diffusion equation can be written as

$$\frac{\partial c_i}{\partial t} = \frac{\partial}{\partial x}\left(D_i \frac{\partial c_i}{\partial x}\right), \tag{2}$$

where t is the diffusion time. When density variation in the system is small, the concentration in Eq. 2 can be replaced by the weight or molar fraction. This practice has been routinely used in studies of diffusion in silicate melts and crystals. When the diffusion coefficient is independent of concentration or spatial coordinate, the diffusion equation takes on the simple expression:

$$\frac{\partial c_i}{\partial t} = D_i \frac{\partial^2 c_i}{\partial x^2}. \tag{3}$$

For diffusion in three-dimensional isotropic media, the diffusion equation takes on the more general form in a Cartesian coordinate:

$$\frac{\partial c_i}{\partial t} = D_i\left(\frac{\partial^2 c_i}{\partial x^2} + \frac{\partial^2 c_i}{\partial y^2} + \frac{\partial^2 c_i}{\partial z^2}\right) = D_i \nabla^2 c_i, \tag{4}$$

where ∇^2 is the Laplacian operator. For diffusion in an axisymmetric sphere, the diffusion equation takes on the special form:

$$\frac{\partial c_i}{\partial t} = D_i\left(\frac{\partial^2 c_i}{\partial r^2} + \frac{2}{r}\frac{\partial c_i}{\partial r}\right), \tag{5}$$

where r is the radial coordinate. Equation 5 can be used to model diffusion in and around mineral grains and fluid or melt inclusions. Equations 2, 3, 4, and 5 are partial differential equations. Their solutions depend on the initial and boundary conditions. Analytical solutions to Eqs. 3, 4, 5, and 6 subject to various initial and boundary conditions can be found in the treatise *The Mathematics of Diffusion* (Crank 1975). For a variable diffusion coefficient, the diffusion

equation can be solved numerically using a finite difference method (Crank 1975).

Fick's laws of diffusion were originally developed for diffusion in fluids. These laws are directly applicable to diffusion in isotropic media such as melts, glasses, and minerals of isometric crystal system. The diffusion coefficient in an isotropic medium is independent of direction or orientation and can be treated as a scalar. For diffusion in anisotropic media, such as minerals of crystal systems other than isometric, the diffusion coefficient will depend on the direction of diffusion in the crystals. Diffusivities measured along different directions in the crystal may be different depending on the symmetry of the crystal. For example, for oxygen diffusion in quartz, Giletti and Yund (1984) found that diffusivities of oxygen parallel and perpendicular to the c axis of quartz differ by two orders of magnitude. Diffusion modeling in such systems may be simplified by using two diffusivities in the cylindrical coordinate:

$$\frac{\partial c_i}{\partial t} = D_{\perp c}\left(\frac{\partial^2 c_i}{\partial r^2} + \frac{1}{r}\frac{\partial c_i}{\partial r}\right) + D_{\parallel c}\frac{\partial^2 c_i}{\partial z^2}, \tag{6}$$

where $D_{\perp c}$ and $D_{\parallel c}$ are diffusivities perpendicular and parallel to the c axis of quartz. Equation 6 can be used to model diffusion in hexagonal, tetragonal, and trigonal crystal systems. For diffusion in orthorhombic crystal systems, diffusion coefficients measured along three orthogonal directions are needed to completely describe a diffusive flux. Shea et al. (2015) presented an example of three-dimensional numerical modeling of anisotropic Fe-Mg diffusion in olivine, which is a mineral in the orthorhombic crystal system. In general, a full description of the direction-dependent diffusivity for diffusion in anisotropic media requires a symmetric second order tensor (Nye 1985). In practice, due to the lack of sufficient diffusion data and complicated geometry of the crystals, simplifications are made in diffusion modeling of anisotropic minerals, for example, by using Eq. 2 or 5 with a single diffusion coefficient (Zhang 2010; Shea et al. 2015). A list of diffusion tensors for different crystal systems can be found in Nye (1985) and Zhang (2010).

Types of Diffusion

Depending on the chemical state of the system, the nature of the diffusants, the initial and boundary conditions, and simplifications involved, several types of diffusion can be identified: self diffusion, chemical diffusion, multicomponent diffusion, effective binary diffusion, thermal diffusion, and grain boundary diffusion.

Self diffusion or tracer diffusion takes place when the system of interest is at chemical, but not isotopic, equilibrium. There is no concentration or chemical potential gradient of any elements in the system. Self diffusivity of an element or component is determined by labeling some of the atoms in the diffusant using isotopic tracers, hence the name tracer diffusion. For example, to determine the self diffusivity of Mg in an olivine crystal, one can deposit a thin layer of ^{26}Mg-spiked olivine on the surface of the crystal and follow the spread of ^{26}Mg in the olivine grain.

Chemical diffusion or multicomponent diffusion takes place when the system of interest is out of chemical equilibrium. Many geological systems are made of two or more components. A silicate magma, for example, typically has seven or more major oxide components. Diffusion in such systems is referred to as multicomponent diffusion or chemical diffusion. During chemical diffusion, the concentration gradient of one component may affect the diffusive flux of another component. Lars Onsager generalized Fick's laws of diffusion in binary fluids to multicomponent systems by considering the rate of entropy production which can be written as a sum of scalar products between diffusive fluxes and driving forces for diffusion (e.g., de Groot and Mazur 1962; Hasse 1969). The driving force for chemical diffusion at a constant temperature and pressure is the chemical potential gradient. Since chemical potential of a component in a multicomponent substance (μ_i) is a function of temperature, pressure, and concentration, it is convenient to express diffusive fluxes in terms of concentration gradients of the components in the system. For a binary fluid, for example, Fick's first law can be written as

$$\mathbf{J_i} = -L_i\frac{\partial \mu_i}{\partial x} = -\left(L_i\frac{\partial \mu_i}{\partial c_i}\right)\frac{\partial c_i}{\partial x}, \tag{7}$$

where L_i is the phenomenological coefficient for diffusion. The term in the parentheses is identified as the diffusion coefficient. According to Onsager (1945), the diffusive flux of a given component in a multicomponent liquid can be expressed as a linear combination of concentration gradients of the independent components in the system. In a volume-fixed frame of reference, the one-dimensional diffusive flux of component i in an n component fluid or melt at constant temperature and pressure is given by (Onsager 1945):

$$\mathbf{J_i} = -\sum_{j=1}^{n-1} D_{ij}\frac{\partial c_j}{\partial x}, \tag{8}$$

where D_{ij} are elements of an $(n-1)$ by $(n-1)$ diffusion matrix with component n taken as the dependent variable. The index i in Eq. 8 takes on integers $1, 2, \ldots, n-1$. The diffusive flux of the dependent component n is constrained by the requirement of total flux conservation. The latter depends on the choice of reference frame. An important property of the diffusion matrix is that its eigenvalues are positive, which is

a prerequisite for stable solutions of the diffusion equations. For a ternary system, there are two independent components. The diffusion equations for the independent components 1 and 2 are

$$\frac{\partial c_1}{\partial t} = D_{11}\frac{\partial^2 c_1}{\partial x^2} + D_{12}\frac{\partial^2 c_2}{\partial x^2}, \tag{9a}$$

$$\frac{\partial c_2}{\partial t} = D_{21}\frac{\partial^2 c_1}{\partial x^2} + D_{22}\frac{\partial^2 c_2}{\partial x^2}, \tag{9b}$$

where D_{11} and D_{22} are the diagonal terms and D_{12} and D_{21} are the off-diagonal terms of the 2 × 2 diffusion matrix. For diffusion in an n component system, the diffusion equation for component i is

$$\frac{\partial c_i}{\partial t} = \sum_{j=1}^{n-1} D_{ij}\frac{\partial^2 c_j}{\partial x^2}. \tag{10}$$

Equations 9 and 10 are coupled diffusion equations because of the presence of the off-diagonal terms. A peculiar consequence of coupled diffusion is uphill diffusion, which happens when the spreading direction of a diffusant is in the opposite direction of its own concentration gradient (i.e., the diffusant can migrate from regions of low concentration to high concentration). Uphill diffusion is a transient phenomenon. It occurs when the net diffusive flux produced by concentration gradients of all other components in Eq. 10 is larger than and has the opposite sign relative to the diffusive flux produced by the concentration gradient of the component of interest. Examples of uphill diffusion in molten silicates can be found in Zhang et al. (1989), Watson and Baker (1991), Liang et al. (1996), Richter et al. (1998), and Guo and Zhang (2016). When elements of the diffusion matrix are constant and uniform, analytical solutions to the coupled diffusion equations can be constructed from solutions to the equivalent binary cases using the method of linear transformation (Toor 1964; Gupta and Cooper 1971). Exact solutions for multicomponent diffusion in ternary systems were derived by Fujita and Gosting (1956) and Kirkaldy (1958) for one-dimensional semi-infinite diffusion couples. A recent summary with additional examples can be found in Liang (2010).

Numerical values of the diffusion matrix depend on the choice of the dependent variable, units of concentration, and the frame of reference for the diffusive fluxes. The volume-fixed frame of reference is most suitable for studying chemical diffusion in the laboratory. For diffusive mass transfer in geological systems, mass-fixed frame of reference is most convenient. The difference between the two frames of reference is whether the sum of the volume fluxes or the mass fluxes is set to zero. For a general treatment of multicomponent diffusion, including coordinate transformation, the reader is referred to the textbooks or monographs by de Groot and Mazur (1962), Katchalsky and Curran (1967), Hasse (1969), Tyrrell and Harris (1984), Miller et al. (1986), Kirkaldy and Young (1987), and Kondepudi and Prigogine (1998). Relevant reviews or summaries in the geochemical literature include Anderson (1981), Lasaga (1998), and Liang (2010).

Effective binary diffusion is a simplified treatment of chemical diffusion in multicomponent fluids or solids. Here the multicomponent system is treated as a pseudo-binary system in which the component of interest is taken as the independent variable and all other components are taken together as the dependent variable (Cooper 1968). The diffusive flux of the component of interest (i) is assumed to follow a relation similar to Fick's first law of diffusion for binary fluids,

$$\mathbf{J_i} = -D_i^E\frac{\partial c_i}{\partial x}, \tag{11}$$

where D_i^E is the effective binary diffusion coefficient of component i. The diffusive flux defined by Eq. 11 is equivalent to that defined by Eq. 8 if the effective binary diffusion coefficient is given by (Cooper 1968):

$$D_i^E = \sum_{j=1}^{n-1} D_{ij}\frac{\partial c_j}{\partial c_i}. \tag{12}$$

Most diffusion coefficients for chemical diffusion in fluids, melts, and crystals reported in the geochemical literature were obtained using the effective binary approximation (see reviews by Watson and Baker 1991; Zhang et al. 2010). Unlike the diffusion matrix for a multicomponent system, the effective binary diffusion coefficients depend on the direction of diffusion in composition space, that is, they are sensitive to the specific diffusion experiments from which they are derived. This is shown by the composition derivatives in Eq. 12 and verified by many laboratory studies of chemical diffusion in molten silicates. For diffusion in a confined system or finite geometry, $\partial c_j/\partial c_i$ in Eq. 12 may change its sign during diffusion (Watson and Baker 1991; Liang 2010), and the effective binary diffusion coefficient may also vary as a function of time. Since D_i^E must be positive for the diffusion equation to be stable, Eq. 11 cannot be used to model uphill diffusion without additional assumptions (Richter 1993; Zhang 1993). For a detailed discussion on the usefulness and limitations of effective binary diffusion and its relation to multicomponent diffusion, the reader is referred to Cooper (1968), Liang (2010), and Zhang (2010).

Relationship between self diffusion and chemical diffusion Self diffusivity is a measure of the intrinsic mobility of the diffusing species. In the presence of chemical potential or

concentration gradient in a binary system, the intrinsic diffusivity for component 1 (D_1^I) is related to the self diffusivity of component 1 (D_1) through the expression

$$D_1^I = \left(1 + \frac{d\ln\gamma_1}{d\ln X_1}\right) D_1, \tag{13}$$

where γ_1 is the activity coefficient and X_1 is the molar fraction of component 1 in the binary system. The term in the parentheses is called the thermodynamic factor, which is identical to that for component 2 in the binary system. For chemical diffusion in a simple binary fluid or solid, the interdiffusion coefficient ($\tilde{D}$) is related to the intrinsic diffusion coefficients of the two components through Darken's equation

$$\tilde{D} = X_2 D_1^I + X_1 D_2^I = (X_2 D_1 + X_1 D_2)\left(1 + \frac{d\ln\gamma_1}{d\ln X_1}\right). \tag{14}$$

A comparable expression for interdiffusion of two counter ion species in a binary crystal or fluid is given by the expression (Helfferich and Plesset 1958; Barrer et al. 1963):

$$\tilde{D} = \frac{D_1 D_2 (X_1 Z_1^2 + X_2 Z_2^2)}{D_1 X_1 Z_1^2 + D_2 X_2 Z_2^2}\left(1 + \frac{d\ln\gamma_1}{d\ln X_1}\right), \tag{15}$$

where Z_1 and Z_2 are charge numbers of the two ions. When the abundance of component 1 is much smaller than that of component 2 ($X_1 << X_2$), the interdiffusion coefficient in Eq. 14 or 15 is mostly determined by the self diffusivity of component 1. Generalizations of Eqs. 14 and 15 to multicomponent geological fluids or solids can be found in Cooper (1965), Lasaga (1979), and Liang et al. (1997). In all cases, the diffusion matrix can be written as a product of a kinetic matrix and a thermodynamic matrix. Elements of the kinetic matrix are functions of self diffusivities of the components in the system, while elements of the thermodynamic matrix depend on activity-composition relationships of the components. Darken's equation and its generalizations have been used to study chemical diffusion in molten silicates and selected minerals (Chakraborty 2010; Ganguly 2010; Liang 2010).

Thermal diffusion is a general case of chemical diffusion in that the flow of heat drives a flow of matter. This transport phenomenon is often referred to as the "Soret effect" after the Swiss chemist Charles Soret. The driving force for thermal diffusion involves temperature gradient. For a multicomponent fluid, the diffusive flux for an independent component takes on a more general form (e.g., de Groot and Mazur 1962; Hasse 1969). With concentration in mass fraction, the diffusive flux for component 1 in a binary fluid is written as the sum of two parts – one proportional to the concentration gradient and the other proportional to the temperature gradient:

$$\mathbf{J}_1 = -\rho D_1 \left[\frac{\partial w_1}{\partial x} + S_T w_1 (1 - w_1)\frac{\partial T}{\partial x}\right], \tag{16}$$

where ρ is the density of the fluid; w_1 is the mass fraction of component 1 in the fluid; D_1 is the diffusion coefficient of component 1; and S_T is the Soret coefficient. The product $D_1 S_T$ is called the thermal diffusion coefficient, designated as D_T. The Soret coefficient or thermal diffusion coefficient can be either positive or negative, depending on the response of the component to the imposed temperature gradient. While the concentration gradient serves to homogenize a fluid, the presence of a temperature gradient across the fluid can result in mass separation. This is a key difference between thermal diffusion and chemical diffusion and can be demonstrated by setting the diffusive flux to steady state (i.e., $\mathbf{J}_1 = 0$ in a confined system). Equation 16 then is reduced to

$$\frac{dw_1}{dT} = -w_1(1 - w_1)S_T. \tag{17}$$

For steady-state thermal diffusion across molten silicates, it has been observed in the laboratory that SiO_2, Na_2O, and K_2O migrate towards the hot end (negative S_T), whereas CaO, MgO, FeO, and TiO_2 concentrate towards the cold end (positive S_T) of diffusion charges (Walker et al. 1981; Lesher 1986; Richter et al. 2009).

Grain boundary diffusion is a general case of diffusion in crystalline solids in which the boundaries between neighboring grains and dislocation pipes within the crystals serve as fast-pathways or short-circuits for the spreading of diffusant. Diffusion in polycrystalline materials is multipath and consists of both lattice diffusion (also called volume diffusion) and grain boundary diffusion. The mathematical treatment of diffusion in polycrystalline materials generally requires two independent diffusivities, one for diffusion in the crystal lattice and the other for diffusion along grain boundaries or dislocation pipes (Fisher 1951; Whipple 1954; Suzuoka 1961; Le Claire 1963). The structure of grain boundaries are relatively open compared to the structure of the crystal lattice. Diffusion along grain boundaries is typically orders of magnitude faster than diffusion within the crystal lattice. The grain boundary diffusivity is comparable to the diffusivity in the melt as the temperature approaches the melting temperature of the solid (Mishin et al. 1997). During diffusion, a particle may spend some fraction of time in the crystal lattice and the rest of the time in the grain boundary, wandering back and forth between the lattice and the grain boundary. Depending on their relative contributions to the bulk or net transport of diffusants through the polycrystalline material, three types or regimes of grain boundary diffusion are identified in the absence of grain boundary migration (Harrison 1961): A, B, and C. Types A and C are endmember cases in which volume diffusion is either dominant or insignificant, respectively,

whereas Type B is the intermediate regime and also the most complicated case of grain boundary diffusion. Type C diffusion happens when the diffusion time is too short for appreciable contribution of lattice diffusion, and the net mass transport of diffusants through the polycrystals can be solely accounted for by diffusion along grain boundaries. Type A diffusion is dominant when the diffusion time is long and the volume diffusivity (D_L) is large such that the diffusion length in the solid is much larger than the average grain size (d), that is,

$$\sqrt{D_L t} >> d. \tag{18}$$

The bulk diffusive flux in the polycrystalline material can be modeled by Fick's first law of diffusion (Eq. 1) with an effective diffusion coefficient (D_{eff}) that is a weighted average of diffusivities for the lattice and grain boundary diffusion (Hart 1957):

$$D_{eff} = f_{gb} D_{gb} + \left(1 - f_{gb}\right) D_L, \tag{19}$$

where D_{gb} is the grain boundary diffusivity; f_{gb} is the volume fraction of grain boundaries in the polycrystals. f_{gb} is proportional to the ratio between the grain boundary width and the average grain size. The boundary width is reasoned to be very small, on the order of several interatomic distances. Hence, grain boundary diffusion is more effective for diffusive mass transfer in fine-grained solids (larger f_{gb}) at low temperatures (smaller D_L). Type B regime is observed when significant concentration zoning is present in the crystals. The diffusion length in the crystal is smaller than the grain size. Depending on temperature, diffusion time, and grain size, the three regimes of grain boundary diffusion may coexist in different parts of a system. During grain growth or recrystallization, grain boundaries migrate in polycrystalline solids. The classification of grain boundary diffusion also depends on the grain boundary migration velocity. For additional reading on grain boundary diffusion, including mathematical treatment and summary of diffusion data in silicate and oxide minerals, the reader is referred to the review articles by Joesten (1991), Mishin et al. (1997), Watson and Baxter (2007), and Dohmen and Milke (2010).

Diffusion Coefficients

Diffusion is a thermally activated process. In general, both self diffusion and chemical diffusion coefficients in a substance or medium vary systematically with temperature, pressure, and composition. For a given composition, the diffusion coefficient of a component (D) in the medium follows the Arrhenius equation:

$$D = D_0 \exp\left(-\frac{E_a + PV_a}{RT}\right), \tag{20}$$

where D_0 is the pre-exponential factor for diffusion (in $m^2\ s^{-1}$); E_a is the activation energy for diffusion (in J mol^{-1}); V_a is the activation volume for diffusion (in $m^3\ mol^{-1}$); T is the temperature (in K); P is the pressure (in Pa); and R is the gas constant (8.314 J $mol^{-1}\ K^{-1}$). D_0 is related to the vibration frequency and jumping distance of the diffusing species in the medium. The sum $E_a + PV_a$ in the Arrhenius equation is called the activation enthalpy for diffusion (H_a). The linearized version of the Arrhenius equation can be used to determine the diffusion parameters (D_0, E_a, and V_a):

$$\ln D = \ln D_0 - \frac{E_a + PV_a}{RT}. \tag{21}$$

A set of diffusion coefficients of a component in the medium measured at a constant pressure but different temperatures generally defines a straight line in the plot of ln D against the reciprocal of the temperature (Fig. 1). Such a diagram is referred to as the Arrhenius plot or Arrhenius diagram. The intercept of the line is ln D_0 and the slope of the line in the Arrhenius plot is $-H_a/R$. The larger the activation energy for diffusion, the stronger the dependence of diffusion on temperature. The activation enthalpy obtained through a set of

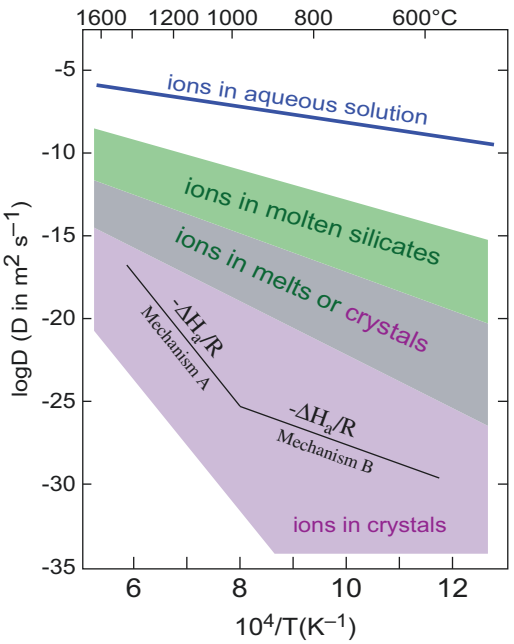

Diffusion, Fig. 1 Arrhenius plot illustrating the ranges of diffusivities of various cations and anions in aqueous solutions, molten silicates, and crystals. The change in the slope in this diagram may indicate a change in diffusion mechanism (A vs. B) (Modified from Watson and Baxter (2007) by E. Bruce Watson)

diffusion data collected at a constant pressure is often called the activation energy in the literature, which may cause confusion. Care should be exercised when comparing activation energies measured at different pressures. Deviation from the straight line in the Arrhenius plot, such as a change in the slope (black lines in Fig. 1), often suggests either a change in diffusion mechanism or inaccurate diffusion data. A family of straight lines is established in the Arrhenius plot if diffusion coefficients are measured over a range of pressures and temperatures. A comprehensive compilation of diffusivities and diffusion parameters for self diffusion and chemical diffusion of cations, anions, volatile species, and noble gases in silicate melts and crystals can be found in the monograph *Diffusion in Minerals and Melts* (Zhang and Cherniak 2010). A few first order features are highlighted below.

Depending on physical state of the substance and diffusing species, values of activation energy for diffusion in earth and planetary materials vary greatly. In general, diffusivities of ions (cations and anions) in aqueous solutions are considerably larger than those in molten silicates which, in turn, are larger than those in silicate or oxide minerals. Activation energies for diffusion in the minerals are generally larger than those for diffusion in the melts with which the minerals may reside (e.g., olivine and pyroxene vs. basalts, feldspars vs. rhyolites). Figure 1 is from Watson and Baxter (2007) and illustrates the enormous ranges of diffusivity and activation enthalpy for diffusion of cations and anions in geological fluids, melts, and minerals, from ~40 kJ mol^{-1} for interdiffusion in supercritical aqueous solution (Wark and Watson 2004) up to ~800 kJ mol^{-1} for tetravalent Hf diffusion in zircon (Cherniak et al. 1997a). Figure 2 highlights both the complexity and systematics of the Arrhenius relations for monovalent (H, Li, Na, and K), divalent (Ca and O), tetravalent (Ti and Si) ions and molecules (H_2O and Ar) in quartz under nominally anhydrous conditions. The general trends of increasing activation energy and decreasing diffusivity with increasing ionic charge and size are also observed for diffusion in other minerals and silicate melts, although exceptions are abundant. For example, diffusivities of trivalent REE in diopside and zircon vary systematically as a function of ionic radius (Cherniak et al. 1997b; Van Orman et al. 2001), whereas diffusivities of REE in enstatite and plagioclase appear to be insensitive to the size of REE (Cherniak 2003; Cherniak and Liang 2007).

Few studies have focused on the effect of pressure on cation diffusion in minerals and melts, as pressure has a negligible effect on diffusion under crustal conditions. However, pressure may play an important role in modulating diffusion rate under mantle conditions. For example, diffusivities of network-forming cations, such as Si and Al, in

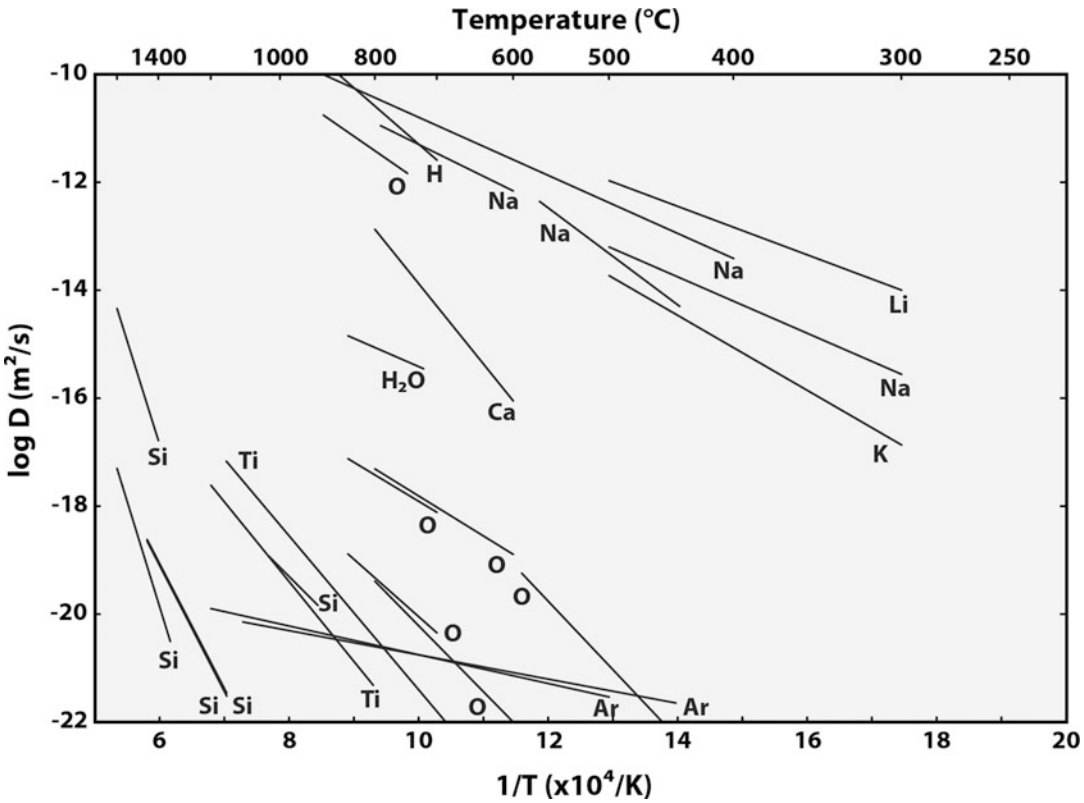

Diffusion, Fig. 2 Diagram summarizing Arrhenius relations for diffusion of various cations, anions (oxygen), and Ar in quartz under nominally anhydrous conditions (Adapted from Brady and Cherniak 2010)

highly polymerized melts increase with the increase of pressure (an apparent negative activation volume), which are attributed to changes in the melt structure with pressure (Kushiro 1983; Poe et al. 1997). Activation volumes (V_a) for cation diffusion in minerals are generally positive and range from less than 10^{-6} m^3 mol^{-1} to 20×10^{-6} m^3 mol^{-1} (Béjina et al. 2003; Chakraborty 2010). At 1200 °C, trivalent REE diffusivities in diopside (V_a ~10×10^{-6} m^3 mol^{-1}, Van Orman et al. 2001) and garnet ($V_a = 10 \times 10^{-6}$ to 20×10^{-6} m^3 mol^{-1}, Van Orman et al. 2002; Carlson 2012; Bloch et al. 2015) decrease by one and two orders of magnitude, respectively, when the pressure is increased from 1 to 4 GPa. The diffusion of divalent cations (Fe-Mg, Mn, and Ni) in garnet and olivine depends moderately on pressure ($V_a = 4\sim8 \times 10^{-6}$ m^3 mol^{-1}, Béjina et al. 2003; Holzapfel et al. 2007; Chakraborty 2010). Since diffusion coefficients decrease with the decrease of temperature and the increase of pressure, simultaneous changes in temperature and pressure along a geotherm can significantly reduce temperature-induced variations in diffusivity (Holzapfel et al. 2007; Watson and Baxter 2007; Liang 2017). Holzapfel et al. (2007) gave an example of Fe-Mg diffusion in olivine along a *P-T* path in the upper mantle. According to their calculation, the diffusivity of Fe-Mg in olivine increases from ~10^{-25} to 10^{-15} m^2 s^{-1} in the lithosphere (50–150 km depth) and then decreases gradually through the asthenosphere. Near the bottom of the upper mantle (400 km) the Fe-Mg diffusion coefficient is reduced to 10^{-16} m^2 s^{-1}. Without the competing effect of pressure, the Fe-Mg diffusivity in olivine would monotonically increase in the asthenospheric part of the upper mantle. Similar variations in diffusivity with depth are also expected for cation diffusion in other mantle minerals (Watson and Baxter 2007).

Diffusion in oxides and silicate crystals depends on diffusion mechanism and defect chemistry (Watson and Baxter 2007; Chakraborty 2008, 2010; Cherniak and Dimanov 2010; Van Orman and Crispin 2010). The mechanisms of diffusion in minerals are complicated and still not well understood in many cases. Because natural minerals typically are solid solutions and contain vacancies and impurities of various sizes and valences, diffusion of an ion in a mineral may take more than one mechanism. For the same ion, its diffusion mechanism in one mineral may not necessarily be the same as in another mineral. For example, Li diffusion in olivine follows two pathways: a fast path through interstitial sites and a slow path through octahedral sites in olivine (Dohmen et al. 2010), whereas Li diffusion in zircon appears to follow one mechanism (Cherniak and Watson 2010; Trail et al. 2016). When vacancies are involved, diffusion in minerals can be broadly divided into two regimes: a high temperature or intrinsic regime where diffusivity is proportional to vacancy abundance in the minerals, and a low temperature or extrinsic regime where the vacancy abundance is low and does not contribute significantly to the overall diffusion. For Fe-bearing minerals, vacancy abundance is sensitive to oxygen fugacity. Measured diffusivities then depend on oxygen fugacity (e.g., Fe-Mg diffusion in olivine, Chakraborty 2010). The activation enthalpy for diffusion in the intrinsic regime is higher than that for diffusion in the extrinsic regime. The two regimes of diffusion are illustrated as mechanisms A and B in Fig. 1. Diffusion in minerals also depends on mineral composition. Cation diffusion in feldspars, for example, is very sensitive to feldspar compositions: Mg, Pb, Sr, and Nd diffusivities in anorthite are one to two orders of magnitude smaller than those in oligoclase (Giletti and Casserly 1994; Cherniak and Watson 1994; Cherniak 1995, 2003; Van Orman et al. 2014). Finally, the presence of water and H species in minerals enhances oxygen diffusion but generally has very little effect on cation diffusion in minerals (Watson and Baxter 2007). Figure 3 is a broad-brush summary of cation and anion diffusion in minerals commonly observed in the earth and planetary materials (Brady and Cherniak 2010). The general trends and variations in diffusivities highlight the importance of mineral composition, mineral structure, temperature, and oxygen fugacity on diffusion in minerals.

Diffusion in silicate melts depends strongly on melt composition and melt structure (Watson and Baker 1991; Lesher 2010; Liang 2010; Zhang et al. 2010). Chemical diffusivities for cations in silicate melts are typically measured with metal oxides as independent components. In general, diffusivities decrease with the increase of SiO_2 and the decrease of alkali and water contents in the melt. For example, diffusivities of oxide components (including total water) decrease by over an order of magnitude from basalt to rhyolite, whereas the diffusivity of Li_2O only decreases by a factor of two and the diffusivity of CO_2 appears to be insensitive to melt composition (Watson and Baker 1991; Richter et al. 2003; Zhang and Ni 2010). Figure 4 displays an example of chemical diffusion between a basaltic melt and a rhyolitic melt (Richter et al. 2003). The steep gradients on the high SiO_2 or rhyolite side of the diffusion couple are due to the composition-dependent diffusivity in the melt, and can be reproduced by allowing the effective binary diffusion coefficients of the oxides to vary by factors of ~10–20 across the diffusion couple (Richter et al. 2003).

It has been demonstrated experimentally that isotopes of a number of elements (Li, Mg, Ca, K, Fe, and Ge) can be fractionated from each other during self diffusion, chemical diffusion, and thermal diffusion in aqueous solutions, molten silicates, iron-nickel alloys, as well as minerals such as pyroxene (e.g., Richter et al. 1999, 2003, 2006, 2009, 2014, 2016; Watkins et al. 2011, 2014; Watson et al. 2016). Richter and coworkers quantified this effect by relating diffusivity ratio of two isotopes to the reciprocal of their mass ratio through an empirical kinetic parameter β:

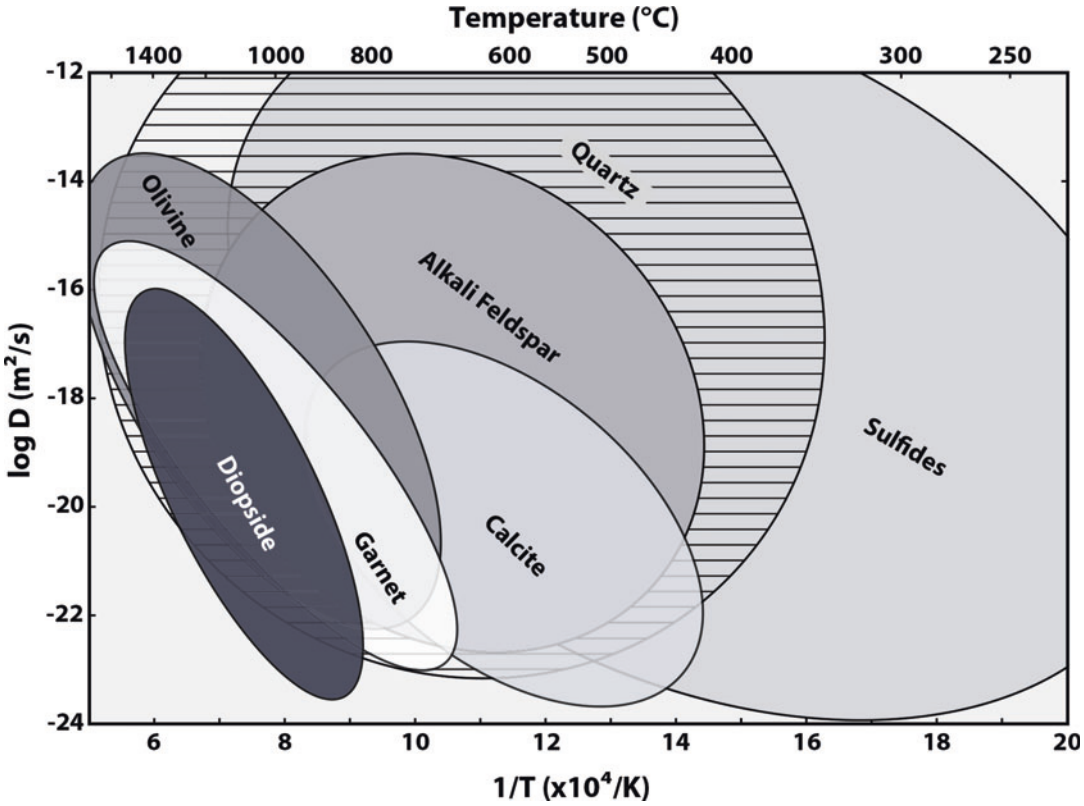

Diffusion, Fig. 3 Schematic Arrhenius diagram showing the approximate ranges of measured diffusion coefficients and temperatures for all elements (except H, He, Ar, and Li) in several common minerals or mineral groups (Adapted from Brady and Cherniak 2010)

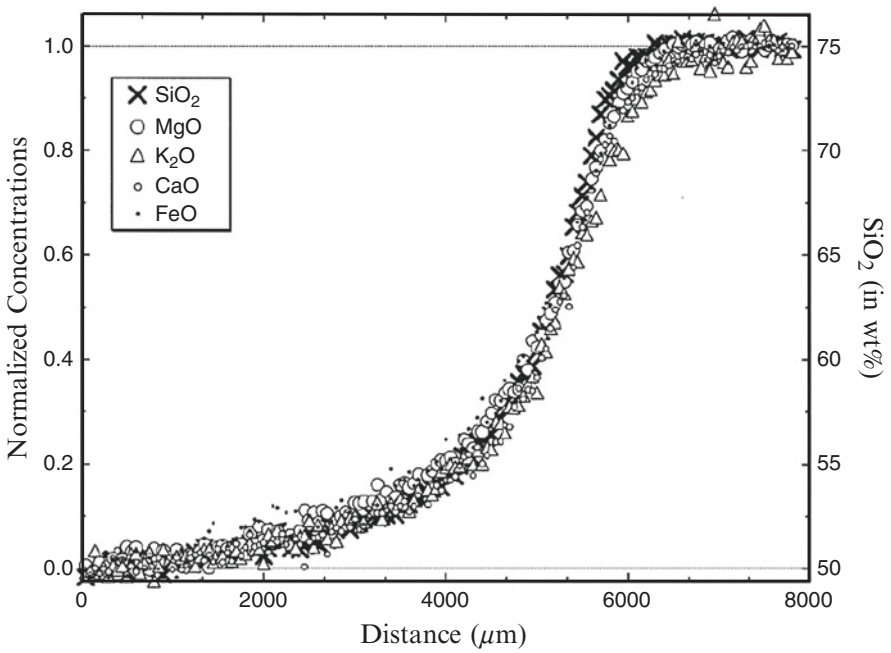

Diffusion, Fig. 4 Variations of selected oxide abundances across a basalt-rhyolite diffusion couple. The diffusion experiment was conducted at 1450 °C and 1.3 GPa for 15.7 h. At the start of the experiment, compositions of the basalt (left) and rhyolite (right) are homogeneous and shown as thin gray lines. The measured concentration profiles are shown as open circles. The small dots are calculated diffusion profiles using composition-dependent effective binary diffusion coefficients (Adapted from Richter et al. 2003)

$$\frac{D_1}{D_2} = \left(\frac{M_2}{M_1}\right)^{\beta}, \tag{22}$$

where D is the diffusivity and M is the mass of isotope 1 or 2 of the element of interest. While the experimentally determined β values in silicate melts are small for cations (0.215 for Li, but <0.1 for Ca, Mg, Fe and Si), they give rise to kinetic isotope fractionations that are larger compared to the precision with which isotope ratios are routinely measured. The values of {\beta} in minerals are often larger than in melts (e.g., ~0.3 for Li in pyroxene), while they are much smaller for salts diffusing in water. But in every case the light isotope diffuses slightly faster than the heavy isotope. Compilations of β values in aqueous solutions, melts, and minerals can be found in Richter et al. (2009) and Watkins et al. (2017). Isotope fractionation by diffusion is becoming a powerful tool for identifying diffusion-dominated mass transfer process in natural samples and as a result there is a growing interest in its geochemical applications. Some examples involving measurements and diffusion modeling of both isotopic ratio and element concentration profiles in natural settings can be found in Teng et al. (2006), Chopra et al. (2012), Sio et al. (2013), and Richter et al. (2014, 2016), among others.

Methods for Measuring Diffusion Coefficients

Diffusion coefficients for earth and planetary materials reported in the literature are mostly obtained from laboratory experiments. The methods for measuring diffusivities vary considerably, depending on physical state of the matter (fluid, melt, glass, or solid) and availability of analytical methods. Regardless of experimental complexity and sophistication, the basic idea of all diffusion experiments remain the same: Given an initial perturbation in concentration or isotopic ratio on the surface or in part of the specimen of interest, monitor the spread of the diffusant in the specimen as a function of diffusion time by measuring concentration and/or isotopic ratio profile(s) in the experimental charge using a suitable analytical instrument, and retrieve diffusion coefficient(s) from the measured concentration profiles using solutions to diffusion equations pertinent to the experimental setup. For the convenience of mathematical treatment of diffusion data, diffusion experiments are typically arranged in an effective one-dimensional geometry using one of the three setups or methods: diffusion couple method, thin source method, and constant source method. In the diffusion couple method, two rods or slabs of uniform but different composition starting materials are juxtaposed against each other in a capsule. In the thin source method, a thin film of diffusant is deposited on the surface of a polished specimen. In the constant source method, concentration of the diffusant at the surface or interface of the specimen of interest is kept constant during the course of diffusion. The diffusion couple method has been widely used to study self diffusion and chemical diffusion in molten silicates. This method has also been used to study chemical diffusion in minerals (e.g., garnet, olivine, and spinel) that have relatively fast diffusion rates on the laboratory time scale (the high temperature region labeled "ions in melts or crystals" in Fig. 1). The thin source method has been more frequently used to study diffusion in solids (minerals and glasses). The constant source method has been used to study diffusion of trace elements in either melts or minerals. This method has also been used to study diffusional loss or gain of diffusant in mineral grains in spherical geometry. The length of diffusion profile and the abundance of diffusant largely determine the analytical method used in a diffusion study (e.g., electron microprobe, ion microprobe, laser-ablation inductively coupled mass spectrometry, Rutherford backscatter spectroscopy, and nuclear reaction analysis). Depending on diffusivity and experimental run duration (minutes to a month), typical diffusion lengths range from 100s ~1000s microns for diffusion in melts (e.g., basalt-rhyolite interdiffusion) to 10s microns ~ less than 100 nanometers for diffusion in minerals (e.g., Fe-Mg diffusion in olivine; REE diffusion in pyroxene). Experimental studies of diffusion in fluids at elevated temperatures and pressures are more challenging and require special setups and capsules (e.g., the differential solubility and diffusion cell of Watson and Wark 1997; Wark and Watson 2004). A common practice in laboratory diffusion measurements is the time series study, in which a set of diffusion experiments is carried out at the same temperature and pressure but for different annealing times. Diffusion coefficients obtained from a time series study should be identical to within experimental uncertainty if diffusion is the sole mass transfer mechanism. To determine activation energy and activation volume for diffusion, diffusion experiments are conducted over a range of temperatures and pressures. Diffusivities obtained from such experiments can be used to extract diffusion parameters for the Arrhenius equation (Eq. 20). Finally, it is worth noting that diffusivities in fluids, melts, and crystals can be calculated theoretically through atomistic simulations. Computer simulations can extend the temperature and pressure ranges beyond those accessible in the laboratory, making it a powerful tool for studying thermodynamic and transport properties (including diffusivity) of earth and planetary materials. So far, atomistic simulations have been mainly used to study diffusion of major elements in simple but geologically relevant materials and the results are promising. For detailed summaries of various methods used in diffusion studies, the reader is

referred to the review articles by Ryerson (1987), Cherniak et al. (2010), de Koker and Stixrude (2010), and Watson and Dohmen (2010).

Diffusion Length and Closure Temperature

Diffusion length is a measure of the length scale of a region that is affected by the spread of diffusant. The diffusion length, L_D, scales with the square root of diffusion time and is given by the simple expression:

$$L_D = \sqrt{Dt}. \tag{23}$$

For diffusion coefficients $D = 10^{-6}$, 10^{-11}, and 10^{-19} $m^2\,s^{-1}$, which are within the ranges for diffusion in fluids, melts, and solids (Fig. 1), the diffusion lengths are 5.6 km, 18 m, and 1.8 mm, respectively, for a diffusion time of one million years. Depending on time scales of geological processes, concentration variations in mineral grains may not be effectively homogenized by diffusion. Indeed, zoning patterns preserved in mineral grains offer valuable information on time scales of geological processes, such as magma residence time, magma ascent rates, and cooling rates (Dohmen et al. 2017). During cooling, the diffusivity decreases with temperature and time, and the diffusion length may be estimated using a time-integrated diffusivity:

$$L_D = \left[\int_0^t D(t)dt\right]^{\frac{1}{2}}. \tag{24}$$

With decreasing temperature, concentration profiles in the interiors of the mineral grain become progressively insensitive to variations in mineral surface concentration. In terms of diffusional loss or gain, the mineral effectively ceases diffusive exchange with its surrounding at some lower temperature limit. This lower temperature limit is called the closure temperature (Dodson 1973). At closure temperature, the diffusion length defined by Eq. 24 is comparable to mineral grain size. By considering diffusional loss to a large reservoir along a prescribed cooling curve, Dodson (1973, 1986) obtained an equation for the mean closure temperature (T_c) for an element in a mineral grain of effective radius d,

$$\frac{E_a}{RT_c} = G + \ln\frac{D_0RT_c^2}{E_a\dot{s}d^2}, \tag{25}$$

where $\dot{s}$ is the absolute value of cooling rate at the closure temperature; G is the spatial average of the closure function and depends on geometry of the mineral ($G = 4.0066$ for sphere, 3.29506 for cylinder, and 2.15821 for plane sheet). The closure temperature decreases with the decrease of the product of cooling rate and the square of the effective diffusion radius. The geometric function, G, in Dodson's equation was modified by Ganguly and Tirone (1999) to include the "memory effect" that arises from situations when diffusion has not affected the center of the crystal (i.e., cases of fast cooling and/or large grain size). In his original derivation, Dodson (1973) used a cooling curve along which the reciprocal of the temperature increases linearly as a function of time. Generalization of Dodson's equation can be made to other heating-cooling-upwelling scenarios (Gardés and Montel 2009; Watson and Cherniak 2013; Liang 2017) and to two minerals in a closed system (Powell and White 1995; Liang 2015). Combined with geothermometers and isotopic dating, closure temperatures can be used to constrain thermal history of igneous and metamorphic rocks (Mueller et al. 2010).

Summary

Diffusion is a kinetic phenomenon that arises when there are gradients in concentration, chemical potential or temperature in a substance. Many geological processes are rate-limited by diffusion. Fick's laws of diffusion form the basis for quantifying diffusion kinetics in earth and planetary materials. The types of diffusion that are important to understand diffusion kinetics include self diffusion, chemical diffusion, multicomponent diffusion, effective binary diffusion, thermal diffusion, and grain boundary diffusion. Diffusion is a thermally activated process. Diffusion coefficients for geologically relevant fluids, melts, and solids vary enormously and systematically. The temperature- and pressure-dependent diffusivities follow the Arrhenius equation. Diffusion in silicate melts and crystals also depends on composition and structure of the melts and the crystals. Methods for measuring diffusion coefficients depend on physical state of the matter and availability of analytical methods. Atomistic simulations are becoming a powerful tool for diffusion studies and have the potential to significantly improve our knowledge and understanding of diffusion of earth and planetary materials at temperatures and pressures inaccessible in the laboratory. The field of diffusion studies is expanding owing to the continuing improvement and development of experimental, computational, and analytical methods, theories for diffusion, and numerical models for diffusion-related mass transfer. Because the diffusion equations are time-dependent, they can be used to infer rates and time scales of geological processes. There is a growing interest in applying diffusion data and models to field observations of earth and planetary materials. Indeed, diffusion is a cornerstone that connects several branches of the earth and planetary sciences.

Cross-References

- Activation Parameters: Energy, Enthalpy, Entropy, and Volume
- Activity and Activity Coefficients
- Analytical Techniques
- Aqueous Solutions
- Crystal Chemistry
- Electron Probe Microanalysis (EPMA)
- Experimental Mineralogy and Petrology
- Fugacity
- Geothermometry and Geobarometry
- Ion Microprobe
- Ionic Radii
- Kinetics of Geochemical Processes
- Laser Ablation – Inductively Coupled Plasma Mass Spectrometry
- Magmatic Process Modeling
- Mass Transfer
- Metamorphic Reactions and Processes
- Mineral Defects
- Mineralogy
- Silicate Melts
- Silicate Minerals
- Trace Elements

References

Anderson AC (1981) Diffusion in electrolyte mixtures. Rev Mineral 8:211–260

Barrer RM, Bartholomew RF, Rees LVC (1963) Ion exchange in porous crystals. Part II. The relationship between self- and exchange-diffusion coefficients. Phys Chem Solids 24:309–317

Béjina F, Jaoul O, Liebermann RC (2003) Diffusion in minerals at high pressure: a review. Phys Earth Planet Inter 139:3–20

Bloch E, Ganguly J, Hervig R, Cheng W (2015) ^{176}Lu-^{176}Hf geochronology of garnet I: experimental determination of diffusion kinetics of Lu^{3+} and Hf^{4+} in garnet, closure temperatures and geochronological implications. Contrib Mineral Petrol 169:12

Brady JB, Cherniak DJ (2010) Diffusion in minerals: an overview of published experimental diffusion data. In: Zhang Y, Cherniak DJ (eds) Diffusion in minerals and melts. Reviews in mineralogy and geochemistry. Mineralogical Society of America, Chantilly, Virginia, vol 72. pp 899–920

Carlson WD (2012) Rates and mechanism of Y, REE, and Cr diffusion in garnet. Am Mineral 97:1598–1618

Chakraborty S (2008) Diffusion in solid silicates: a tool to trace time-scales of processes comes of age. Annu Rev Earth Planet Sci 36:153–190

Chakraborty S (2010) Diffusion coefficients in olivine, wadsleyite and ringwoodite. In: Zhang Y, Cherniak DJ (eds) Diffusion in minerals and melts. Reviews in mineralogy and geochemistry. Mineralogical Society of America, Chantilly, Virginia, vol 72. pp 603–640

Cherniak DJ (1995) Diffusion of lead in plagioclase and K-feldspar: an investigation using Rutherford backscattering and resonant nuclear reaction analysis. Contrib Mineral Petrol 120:358–371

Cherniak DJ (2003) REE diffusion in feldspar. Chem Geol 193:25–41

Cherniak DJ, Dimanov A (2010) Diffusion in pyroxene, mica and amphibole. In: Zhang Y, Cherniak DJ (eds) Diffusion in minerals and melts. Reviews in mineralogy and geochemistry. Mineralogical Society of America, Chantilly, Virginia, vol 72. pp 641–690

Cherniak DJ, Liang Y (2007) Rare earth element diffusion in natural enstatite. Geochim Cosmochim Acta 71:1324–1340

Cherniak DJ, Watson EB (1994) A study of strontium diffusion in plagioclase using Rutherford backscattering spectroscopy. Geochim Cosmochim Acta 58:5179–5190

Cherniak DJ, Watson EB (2010) Li diffusion in zircon. Contrib Mineral Petrol 160:383–390

Cherniak DJ, Hanchar JM, Watson EB (1997a) Diffusion of tetravalent cations in zircon. Contrib Mineral Petrol 127:383–390

Cherniak DJ, Hanchar JM, Watson EB (1997b) Rare-earth diffusion in zircon. Chem Geol 134:289–301

Cherniak DJ, Hervig R, Koepke J, Zhang Y, Zhan D (2010) Analytical methods in diffusion studies. In: Zhang Y, Cherniak DJ (eds) Diffusion in minerals and melts. Reviews in mineralogy and geochemistry. Mineralogical Society of America, Chantilly, Virginia, vol 72. pp 107–170

Chopra R, Richter FM, Watson EB, Scullard CR (2012) Magnesium isotope fractionation by chemical diffusion in natural settings and in laboratory analogues. Geochim Cosmochim Acta 88:1–18

Cooper AR (1965) Model for multi-component diffusion. Phys Chem Glasses 6:55–61

Cooper AR (1968) The use and limitations of the concept of an effective binary diffusion coefficient for multi-component diffusion. In: Wachtman JB, Franklin AD (eds) Mass transport in oxides. NBS special publication. Mineralogical Society of America, Chantilly, Virginia, vol 296. pp 79–84

Crank J (1975) The mathematics of diffusion. Clarendon, Oxford

de Groot SR, Mazur P (1962) Non-equilibrium thermodynamics. Dover, New York

de Koker N, Stixrude L (2010) Theoretical computation of diffusion in minerals and melts. In: Zhang Y, Cherniak DJ (eds) Diffusion in minerals and melts. Reviews in mineralogy and geochemistry. Mineralogical Society of America, Chantilly, Virginia, vol 72. pp 971–996

Dodson MH (1973) Closure temperature in cooling geochronological and petrological systems. Contrib Mineral Petrol 40:259–274

Dodson MH (1986) Closure profiles in cooling systems. Mater Sci Forum 7:145–154

Dohmen R, Milke R (2010) Diffusion in polycrystalline materials: grain boundaries, mathematical models, and experimental data. In: Zhang Y, Cherniak DJ (eds) Diffusion in minerals and melts. Reviews in mineralogy and geochemistry. Mineralogical Society of America, Chantilly, Virginia, vol 72. pp 921–970

Dohmen R, Kasemann SA, Coogan L, Chakraborty S (2010) Diffusion of Li in olivine. Part I: experimental observations and a multi species diffusion model. Geochim Cosmochim Acta 74:274–292

Dohmen R, Faak K, Blundy JD (2017) Chronometry and speedometry of magmatic processes using chemical diffusion in olivine, plagioclase and pyroxene. In: Teng F-Z, Dauphas N, Watkins JM (eds) Non-traditional stable isotopes. Reviews in mineralogy and geochemistry. Mineralogical Society of America, Chantilly, Virginia, vol 82. pp 535–575

Fisher JC (1951) Calculation of diffusion penetration curves for surface and grain boundary diffusion. J Appl Phys 22:74–77

Fujita H, Gosting LJ (1956) An exact solution of the equations for free diffusion in three-component systems with interacting flows, and its use in evaluation of the diffusion coefficients. J Am Chem Soc 78:1099–1106

Ganguly J (2010) Cation diffusion kinetics in aluminosilicate garnets and geological applications. In: Zhang Y, Cherniak DJ (eds) Diffusion in minerals and melts. Reviews in mineralogy and geochemistry. Mineralogical Society of America, Chantilly, Virginia, vol 72. pp 559–601

Ganguly J, Tirone M (1999) Diffusion closure temperature and age of a mineral with arbitrary extent of diffusion theoretical formulation and applications. Earth Planet Sci Lett 170:131–140

Gardés M, Montel J-M (2009) Opening and resetting temperatures in heating geochronological systems. Contrib Mineral Petrol 158:185–195

Giletti BJ, Casserly JED (1994) Strontium diffusion kinetics in plagioclase feldspars. Geochim Cosmochim Acta 58:3785–3793

Giletti BJ, Yund RA (1984) Oxygen diffusion in quartz. J Geophys Res 89:4039–4046

Guo C, Zhang Y (2016) Multicomponent diffusion in silicate melts: SiO_2-TiO_2-Al_2O_3-MgO-Na_2O-K_2O system. Geochim Cosmochim Acta 195:126–141

Gupta PK, Cooper AR Jr (1971) The [D] matrix for multicomponent diffusion. Physica 54:39–59

Harrison LG (1961) Influence of dislocation on diffusion kinetics in solids with particular reference to the alkali halides. Trans Faraday Soc 57:1191–1199

Hart EW (1957) On the role of dislocations in bulk diffusion. Acta Metall 5:597–597

Hasse R (1969) Thermodynamics of irreversible processes. Dover, New York

Helfferich F, Plesset MS (1958) Ion exchange kinetics. A nonlinear diffusion problem. J Chem Phys 28:418–424

Holzapfel C, Chakraborty S, Rubie DC, Frost DJ (2007) Effect of pressure on Fe-Mg, Ni and Mn diffusion in $(Fe_xMg_{1-x})_2SiO_4$ olivine. Phys Earth Planet Inter 162:186–198

Joesten R (1991) Grain-boundary diffusion kinetics in silicate and oxide minerals. In: Gangule J (ed) Diffusion, atomic ordering, and mass transport. Springer, New York, pp 345–395

Liang Y, Richter FM, and Watson EB (1996) Diffusion in silicate melts: II. Multicomponent diffusion in CaO-$_{Al2O3}$-$_{SiO2}$ at 1500°C and 1 GPa. Geochim Cosmochim Acta 60, 5021-5035

Katchalsky A, Curran PF (1967) Nonequilibrium thermodynamics in biophysics. Harvard University Press, Cambridge, MA

Kirkaldy JS (1958) Diffusion in multicomponent metallic systems: I. Phenomenological theory for substitutional solid solution alloys. Can J Phys 36:899–906

Kirkaldy JS, Young DJ (1987) Diffusion in condensed state. Wiley, New York

Kondepudi D, Prigogine I (1998) Modern thermodynamics: from heat engines to dissipative structures. Wiley, New York

Kushiro I (1983) Effect of pressure on the diffusivity of network-forming cations in melts of jadeitic compositions. Geochim Cosmochim Acta 47:1415–1422

Lasaga AC (1979) Multicomponent exchange and diffusion in silicates. Geochim Cosmochim Acta 43:455–469

Lasaga AC (1998) Kinetic theory in the Earth sciences. Princeton University Press, Princeton

Le Claire AD (1963) The analysis of grain boundary diffusion measurments. Br J Appl Phys 14:351–356

Lesher CE (1986) Effects of silicate liquid composition on mineral-liquid element partitioning from Soret diffusion studies. J Geophys Res 91:6123–6141

Lesher CE (2010) Self-diffusion in silicate melts: theory, observations and applications to magmatic systems. In: Zhang Y, Cherniak DJ (eds) Diffusion in minerals and melts. Reviews in mineralogy and geochemistry. Mineralogical Society of America, Chantilly, Virginia, vol 72. pp 269–309

Liang Y (2010) Multicomponent diffusion in molten silicates: theory, experiments, and geological applications. In: Zhang Y, Cherniak DJ (eds) Diffusion in minerals and melts. Reviews in mineralogy and geochemistry. Mineralogical Society of America, Chantilly, Virginia, vol 72. pp 409–446

Liang Y (2015) Simple models for closure temperature of a trace element in cooling bi-mineralic systems. Geochim Cosmochim Acta 165:35–43

Liang Y (2017) Effect of pressure on closure temperature of a trace element in cooling petrological systems. Contrib Mineral Petrol 172:8

Liang Y, Richter FM, Chamberlin L (1997) Diffusion in silicate melts: III. Empirical models for multicomponent diffusion. Geochim Cosmochim Acta 61:5295–5312

Miller DG, Vitagliano V, Sartorio R (1986) Some comments on multicomponent diffusion: negative main term diffusion coefficients, second law constrains, solvent choices, and reference frame. J Phys Chem 90:1509–1519

Mishin Y, Herzig C, Bernardini J, Gust W (1997) Grain boundary diffusion: fundamentals to recent developments. Int Mater Rev 42:155–178

Mueller T, Watson EB, Harrison TM (2010) Applications of diffusion data to high-temperature earth systems. In: Zhang Y, Cherniak DJ (eds) Diffusion in minerals and melts. Reviews in mineralogy and geochemistry. Mineralogical Society of America, Chantilly, Virginia, vol 72. pp 997–1038

Narasimhan TN (2004) Fick's insights on liquid diffusion. Eos 85:499–501

Nye JF (1985) Physical properties of crystals. Clarendon, Oxford

Onsager L (1945) Theories and problems of liquid diffusion. Ann N Y Acad Sci 46:241–265

Poe BT, McMillan PF, Rubie DC, Chakraborty S, Yarger J, Diefenbacher J (1997) Silicon and oxygen self-diffusivities in silicate liquids measured to 15 Gigapascals and 2800 Kelvin. Science 276:1245–1248

Powell R, White L (1995) Diffusive equilibration between minerals during cooling: an analytical extension to Dodson's equation for closure in one dimension. Geol J 30:297–305

Richter FM (1993) A method for determining activity-composition relations using chemical diffusion in silicate melts. Geochim Cosmochim Acta 57:2019–2032

Richter FM, Liang Y, Minarik WG (1998) Multicomponent diffusion and convection in molten MgO-Al_2O_3-SiO_2. Geochim Cosmochim Acta 62:1985–1991

Richter FM, Liang Y, and Davis AM (1999) Isotope fractionation by diffusion in molten oxides. Geochim Cosmochim Acta 63, 2853–2861

Richter FM, Davis AM, DePaolo DJ, Watson EB (2003) Isotope fractionation by chemical diffusion between molten basalts and rhyolite. Geochim Cosmochim Acta 67:3905–3923

Richter FM, Mendybaev RA, Christensen JN, Hutcheon ID, Williams RW, Sturchio NC, Beloso Jr AD (2006) Kinetic isotope fractionation during diffusion of ionic species in water. Geochim. Cosmochim. Acta, 70:277–289

Richter FM, Watson EB, Mendybaev RA, Dauphas N, Geory B, Watkins J, Valley J (2009) Isotope fractionation of the major elements of molten basalt by chemical and thermal diffusion. Geochim Cosmochim Acta 73:4250–4263

Richter FM, Watson EB, Chaussidon M, Mendybaev RA, Ruscitto D (2014) Lithium isotope fractionation by diffusion in minerals. Part 1: pyroxenes. Geochim Cosmochim Acta 126:352–370

Richter FM, Chaussidon M, Mendybaev RA, Kite E (2016) Reassessing the cooling rate and geologic setting of Martian meteorites MIL 03346 and NWA 817. Geochim Cosmochim Acta 182:1–23

Ryerson FJ (1987) Diffusion measurements: experimental methods. Methods Exp Phys 24A:89–130

Shea T, Costa F, Krimer D, Hammer JE (2015) Accuracy of timescales retrieved from diffusion modeling in olivine: a 3D perspective. Am Mineral 100:2026–2042

Sio CK, Dauphas N, Teng F-Z, Chaussidon M, Helz RT, Roskosz M (2013) Discerning crystal growth from diffusion profiles in zoned olivine by in situ Mg-Fe isotopic analyses. Geochim Cosmochim Acta 123:302–321

Suzuoka T (1961) Lattice and grain boundary diffusion in polycrystals. Trans Jpn Inst Met 2:25–32

Teng F-Z, McDonough WF, Rudnick RL, Walker RJ (2006) Diffusion-driven extreme lithium isotopic fractionation in country rocks of the Tin Mountain pegmatite. Earth Planet Sci Lett 243:701–710
Toor HL (1964) Solution of the linearized equation of multicomponent mass transfer: I. AIChE J 10:448–455
Trail D, Cherniak DJ, Watson EB, Harrison TM, Weiss BP, Szumila I (2016) Li zoning in zircon as a potential geospeedometer and peak temperature indicator. Contrib Mineral Petrol 171:25
Tyrrell HJV (1964) The origin and present status of Fick's diffusion law. J Chem Educ 41:397–400
Tyrrell HJV, Harris KR (1984) Diffusion in liquids. Butterworths, London
Van Orman JA, Crispin KL (2010) Diffusion in oxides. In: Zhang Y, Cherniak DJ (eds) Diffusion in minerals and melts. Reviews in mineralogy and geochemistry. Mineralogical Society of America, Chantilly, Virginia, vol 72. pp 757–825
Van Orman JA, Grove TL, Shimizu N (2001) Rare earth element diffusion in diopside: influence of temperature, pressure, and ionic radius, and an elastic model for diffusion in silicates. Contrib Mineral Petrol 141:687–703
Van Orman JA, Grove TL, Shimizu N, Layne GD (2002) Rare earth element diffusion in a natural pyrope single crystal at 2.8 GPa. Contrib Mineral Petrol 142:416–424
Van Orman JA, Cherniak DJ, Kita N (2014) Magesium diffusion in plagioclase: dependence on composition, and implications for thermal resetting of the ^{26}Al-^{26}Mg early solar system chronometer. Earth Planet Sci Lett 385:79–88
Walker D, Lesher CE, Hays JF (1981) Soret separation of lunar liquid. Proc Lunar Planet Sci 12B:991–999
Wark DA, Watson EB (2004) Interdiffusion of H_2O and CO_2 in metamorphic fluids at ~490 to 690 °C and 1 GPa. Geochim Cosmochim Acta 68:2693–2698
Watkins JM, DePaolo DJ, Ryerson FJ, Peterson BT (2011) Influence of liquid structure on diffusive isotope separation in molten silicates and aqueous solutions. Geochim Cosmochim Acta 75:3103–3118
Watkins JM, Liang Y, Richter FM, Ryerson FJ, DePaolo DJ (2014) Diffusion of multi-isotopic chemical species in molten silicates. Geochim Cosmochim Acta 139:313–326
Watkins JM, DePaolo DJ, Watson EB (2017) Kinetic fraction of non-traditional stable isotopes by diffusion and crystal growth reaction. In: Teng F-Z, Dauphas N, Watkins JM (eds) Non-traditional stable isotopes. Reviews in mineralogy and geochemistry. Mineralogical Society of America, Chantilly, Virginia, vol 82. pp 85–125
Watson EB, Baker DR (1991) Chemical diffusion in magmas: an overview of experimental results and geochemical applications. In: Perchuk LL, Kushiro I (eds) Physical chemistry of magmas. Springer, New York, pp 120–151
Watson EB, Baxter EF (2007) Diffusion in solid-Earth systems. Earth Planet Sci Lett 253:307–327
Watson EB, Cherniak DJ (2013) Simple equations for diffusion in response to heating. Chem Geol 335:93–104
Watson EB, Dohmen R (2010) Non-traditional and emerging methods for characterizing diffusion in minerals and minerals aggregates. In: Zhang Y, Cherniak DJ (eds) Diffusion in minerals and melts. Reviews in mineralogy and geochemistry. Mineralogical Society of America, Chantilly, Virginia, vol 72. pp 61–105
Watson EB, Wark DA (1997) Diffusion of dissolved SiO_2 in H_2O at 1 GPa, with implications for mass transport in the crust and upper mantle. Contrib Mineral Petrol 130:66–80
Watson HC, Richter FM, Liu A, Huss GR (2016) Iron and nickel isotope fractionation by diffusion, with applications to iron meteorites. Earth Planet Sci Lett 451:159–167
Whipple RTP (1954) Concentration contours in grain boundary diffusion. Philos Mag 45:1225–1236
Zhang Y (1993) A modified effective binary diffusion model. J Geophys Res 98:11901–11920
Zhang Y (2010) Diffusion in minerals and melts: theoretical background. In: Zhang Y, Cherniak DJ (eds) Diffusion in minerals and melts. Reviews in mineralogy and geochemistry. Mineralogical Society of America, Chantilly, Virginia, vol 72. pp 5–59
Zhang Y, Cherniak DJ (2010) Diffusion in minerals and melts. Reviews in mineralogy and geochemistry, vol 72. Mineralogical Society of America, Chantilly
Zhang Y, Ni H (2010) Diffusion of H, C, and O components in silicate melts. In: Zhang Y, Cherniak DJ (eds) Diffusion in minerals and melts. Reviews in mineralogy and geochemistry. Mineralogical Society of America, Chantilly, Virginia, vol 72. pp 171–225
Zhang Y, Walker D, Lesher CE (1989) Diffusive crystal dissolution. Contrib Mineral Petrol 102:492–513
Zhang Y, Ni H, Chen Y (2010) Diffusion data in silicate melts. In: Zhang Y, Cherniak DJ (eds) Diffusion in minerals and melts. Reviews in mineralogy and geochemistry. Mineralogical Society of America, Chantilly, Virginia, vol 72. pp 311–408

Dissolved Organic Matter (DOM)

Hilairy Ellen Hartnett
School of Earth and Space Exploration and School of Molecular Sciences, Arizona State University, Tempe, AZ, USA

Definition

Dissolved organic matter is a heterogeneous class of water-soluble compounds that contain reduced (organic) carbon from a variety of biological and geological sources with a wide range of chemical reactivity. Dissolved organic matter is a key component in the biogeochemical cycling of carbon.

Introduction

Dissolved organic matter (DOM) is operationally defined as any organic matter that is able to pass through a filter. It is described in contrast to particulate organic matter (POM) retained on the filter. Traditionally, glass fiber filters with a nominal pore size of 0.7 μm were the standard. Currently, smaller-sized filters (0.2 μm) are often used because they are readily available and they remove most bacteria, which can degrade a DOM sample. DOM is derived from many sources both external and internal to an aquatic system. Dissolved organic matter is a complex mixture of organic molecules made up of carbon, hydrogen, and oxygen as well as the heteroatoms nitrogen, phosphorous, and sulfur; thus DOM comprises dissolved organic carbon, nitrogen, phosphorous, and sulfur. This heterogeneity makes it difficult to define DOM composition. Dissolved organic matter is an important component of the global carbon cycle and is among the most reactive pools of organic material at Earth's surface.

(Hedges 2002; Hansell and Carlson 2015). In marine systems, DOM is the primary currency of the microbial loop as it provides a food and energy source to microbes. DOM also forms complexes with trace metals making the metals more soluble and more bioavailable. In addition, in freshwater systems, DOM influences aqueous geochemistry by contributing to acidification in low-alkalinity, weakly buffered systems; it can also impart color, taste, and odor to drinking water.

Marine dissolved organic carbon concentrations range from very low values in the deep ocean (~40 μM) to very high values (>300 μM) in coastal regions. Pore water DOM values tend to be higher as particulate organic matter (POM) decomposition within sediments can release DOM. In freshwater systems, DOM ranges from 40 to1000 μM and can reach mM levels in the most carbon-rich systems (e.g., wetlands, bogs, and swamps). The reactivity or bioavailability of DOM describes how well this carbon pool can support the growth of microorganisms. Due to its diverse molecular composition DOM can be highly reactive or quite recalcitrant.

Sample Collection and Bulk Quantification

The choice of filter for DOM sampling is important. Glass fiber filters and silver membrane filters are easily cleaned but suffer from large pore sizes and very high cost, respectively. Membrane filters, especially nitrocellulose and polypropylene filters, are inexpensive but often cause significant sample contamination because they leach carbon and are difficult to clean. Polyethersulfone filters (PES, Supor™) are membrane filters that can be cleaned with deionized water and are available with small pore sizes. The choice of filter is dictated by the specific needs of the sample and the environment in which it is collected. Ideally samples should be collected and stored in ashed (500 °C, 4 h) glass containers and stored cold and in the dark to reduce biological modifications of the sample. If samples are to be stored for long periods, acidification or freezing will reduce post-filtration alteration.

Bulk quantification of DOM is achieved by converting the organic molecules to CO_2 followed by infrared detection of the CO_2 molecule. The method requires (1) complete removal of inorganic carbon from the sample and then (2) complete oxidation of the reduced organic carbon. Inorganic carbon removal is achieved by reducing pH to <2, converting carbonate and bicarbonate to carbon dioxide, and sparging to remove CO_2 gas. The oxidation of organic carbon can be achieved by UV (light) or by persulfate (wet chemical), but most modern DOM analyzers rely on oxidation by high-temperature combustion (HTC). The HTC methods generally employ a platina-alumina catalyst and temperatures of ~720 °C, followed by nondispersive infrared detection of the CO_2. Dissolved organic nitrogen (the DOM molecules that contain N in addition to C, H, and O) can be quantified separately via HTC followed by chemiluminescent detection of the NO formed during oxidation.

In the 1980s, DOM analytical methods were plagued by uncertainty surrounding analytical blanks. A broad community intercomparison revealed that careful attention to sample collection and handling techniques, as well as a commitment to uniform use of standard reference materials, allows routine, high-precision (CV ~ 3–5%), accurate measurement of DOM concentrations down to <35 μM (Sharp et al. 2002).

Characterization

The specific molecular composition of DOM is important for understanding its reactivity and fate in the environment. The direct analysis of DOM composition can be challenging due to low concentrations of individual DOM components and the sheer number of molecules represented; however, great advances have been made in the last 20 years. Improvements in isolation and extraction techniques have helped the low concentration problem, but all methods isolate only a fraction of the DOM pool. It is important to recognize that no individual analysis technique can detect 100% of the carbon in a sample at the molecular level. Thus, multiple methods must be applied to fully characterize the classes of carbon compounds present or to quantify all the molecules in a sample. Biological and environmental samples are especially complex (Kujawinski 2011; Moran et al. 2016).

DOM is comprised of a wide range of biomolecules and organic moieties ranging from large bio- and geopolymers to low molecular weight monomers. A single natural dissolved organic matter sample can be comprised of thousands of different molecules (Sleighter and Hatcher 2007). The dominant classes of biomolecules include proteins and nucleic acids, carbohydrates (sugars), lipids (fatty acids, sterols, and alkenes), pigments, and an array of smaller primary and secondary metabolites. In marine systems, fresh, algal-derived DOM reflects the relative distribution of the biomolecules in plankton biomass; however, microbial and photochemical degradation of DOM rapidly obscures the molecular composition because partially degraded molecules become unrecognizable and difficult to classify. In the deep ocean, a majority of the DOM cannot be classified as individual biomolecules because they have been partially degraded and no longer fall into a given analytical window. In terrestrial aquatic systems, similar biomolecules predominate, but there are also significant contributions from degraded, soil-derived carbon and from land plants (lignin, as well as humic and fulvic acids). Dissolved organic matter can also include geological and anthropogenically derived compounds (i.e., petroleum-derived compounds, PAHs, pesticides, detergents and surfactants, pharmaceuticals, and other emerging contaminants).

Analytical methods that have been applied to characterize DOM at the molecular level include spectrophotometric and optical techniques, nuclear magnetic resonance (NMR) spectroscopy, 2D gas chromatography, and a wide array of mass spectrometry techniques with a variety of ionization techniques. Stable carbon and radiocarbon isotope analyses of DOM are also possible and reveal information about carbon source, reactivity, and fate in the environment. Mass spectrometry can be applied to both extracted and derivatized components as well as to bulk DOM. High-resolution mass spectrometry (e.g., FT-ICR MS and ToF-MS techniques) is an especially exciting field as it is now possible to identify virtually all of the molecules present in a given sample. This capability enables true proteomics and metabolomics analyses in complex environmental samples.

Optical techniques for DOM characterization are gaining popularity because they require little sample preparation, they are nondestructive, and they can characterize different pools of organic carbon. These techniques include UV-Vis absorbance and fluorescence spectroscopy. Some compound classes of the dissolved organic matter can absorb light (colored dissolved organic matter, CDOM); these molecules affect light penetration and therefore primary production. Only certain classes of organic molecules, generally those that are aromatic or highly conjugated, are also fluorescent (fDOM). Absorbance spectroscopy can be used to characterize the aromatic fraction of the DOM (e.g., specific UV absorbance at 240 nm, $SUVA_{254}$), which is related to humic content. Fluorescence is emerging as a powerful tool to characterize aromatic/humic components of the DOM as well as moieties that contain tryptophan-like and tyrosine-like fluorescence (Fellman et al. 2010). Modeling approaches (PARAFAC) have been developed that quasi-quantify contributions of different fluorescent components (Stedmon and Bro 2008). It is not yet well known what fraction of the DOM is comprised by CDOM and fDOM, and further research is required to determine how the reactivity of CDOM and fDOM relates to the bulk DOM reactivity.

Importance to the Carbon Cycle and Current Questions

Dissolved organic matter plays a major role in the carbon cycle. The marine DOM pool holds ~700 Pg of carbon, roughly equivalent to the atmospheric pool. This DOM is a fundamental component of the Earth's active carbon cycle, and the wide range in molecules present means that some fractions are labile and readily degraded by microbes, while other fractions are recalcitrant and can persist for thousands of years. The DOM pool is also in dynamic equilibrium with particulate organic carbon (POC), and the sorption of DOM to particles provides a measure of protection from microbial degradation. The specific mechanism of this sorptive protection is not well known.

Questions remain as to what controls DOM accumulation and removal in marine and terrestrial systems and how microbial and abiotic processes affect DOM composition. Terrestrial carbon, once thought to be highly refractory (non-labile), has been shown to be reactive on short timescales (days to weeks) in estuaries. Surface ocean carbon in excess of deep ocean concentrations holds a modern radiocarbon signature (recently produced) but seems to be semi-labile, possibly due to the more limited microbial diversity in surface waters relative to that in deep waters and coastal regions. DOM in surface waters can also be photooxidized which may influence the lability of the DOM. The vast, deep ocean pool of DOM is old, but small additions of labile and semi-labile material do occur upon solubilization of sinking biogenic POM, and this labile carbon may have a "priming" effect that induces DOM degradation. The complexity of dissolved organic carbon is enormous, and our understanding of the detailed cycling of dissolved organic carbon is still quite limited. New approaches that link microbial ecology with high-resolution geochemical analyses and informatics data are necessary to achieve predictive understanding of DOM cycling (Moran et al. 2016).

Summary

Dissolved organic matter is a complex mixture of organic molecules that occupies a central role in Earth's surface carbon cycle. The complexity of DOM composition has made it difficult to characterize at the molecular level, and we are only beginning to understand the interactions among microbes, metabolisms, and dissolved organic matter cycling.

Cross-References

- ▶ Analytical Techniques
- ▶ Biogeochemistry
- ▶ Biological Pump
- ▶ Biomarker: Assessment of Thermal Maturity
- ▶ Biopolymers and Macromolecules
- ▶ Carbon Cycle
- ▶ Carbon Isotopes
- ▶ Complexes
- ▶ Gas Chromatography–Mass Spectrometry (GC–MS)
- ▶ High-Resolution Mass Spectrometry
- ▶ Lipids (Bacteria and Archaea)
- ▶ Nitrogen Cycle
- ▶ Nuclear Magnetic Resonance
- ▶ Organic Geochemistry
- ▶ Phosphorus

References

Fellman JB, Hood E, Spencer RGM (2010) Fluorescence spectroscopy opens new windows into dissolved organic matter dynamics in freshwater ecosystems: a review. Limnol Oceanogr 55:2452–2462

Hansell DA, Carlson CA (eds) (2015) Biogeochemistry of marine dissolved organic matter, 2nd edn. Academic Press, San Diego

Hedges JI (2002) Why dissolved organics matter. In: Hansell DA, Carlson CA (eds) Biogeochemistry of marine dissolved organic matter. Elsevier, London, pp 1–33

Kujawinski EB (2011) The impact of microbial metabolism on marine dissolved organic matter. Annu Rev Mar Sci 3:567–599

Moran MA, Kujawinski EB, Stubbins A, Fatland R, Aluwihare LI, Buchan A, Crump BC, Dorrestein PC, Dyhrman ST, Hess NJ, Howe B, Longnecker K, Medeiros PM, Niggemann J, Obernosterer I, Repeta DJ, Waldbauer JR (2016) Deciphering ocean carbon in a changing world. Proc Natl Acad Sci 113:3143–3151

Sharp JH, Carlson CA, Peltzer ET, Castle-Ward DM, Savidge KB, Rinker KR (2002) Final dissolved organic carbon broad community intercalibration and preliminary use of DOC reference materials. Mar Chem 77:239–253

Sleighter RL, Hatcher PG (2007) The application of electrospray ionization coupled to ultrahigh resolution mass spectrometry for the molecular characterization of natural organic matter. J Mass Spectrom 42:559–574

Stedmon CA, Bro R (2008) Characterizing dissolved organic matter fluorescence with parallel factor analysis: a tutorial. Limnol Oceanogr Meth 6:572–579

Dolomite and Dolomitization

Jennifer A. Roberts
Department of Geology, University of Kansas, Lawrence, KS, USA

Definition

Dolomite is a trigonal–rhombohedral, ordered Ca, Mg carbonate mineral ($CaMg(CO_3)_2$) occurring primarily in sedimentary and metamorphic rocks. Dolomitization is the process in which Mg ions replace Ca ions in a calcium carbonate mineral.

Crystal Structure and Geochemistry

The crystal structure of dolomite is similar to calcite with Mg ions substituting for Ca in every other layer. To accommodate this substitution, due to differences in bond lengths between Ca–CO_3 and Mg–CO_3 (238 pm versus 208 pm, respectively), CO_3 in the Mg layer is uniformly rotated about the threefold axis relative to calcite (Reeder and Wenk 1983).

Stoichiometric dolomite (50:50 $CaCO_3$:$MgCO_3$) is part of a solid solution between calcite ($CaCO_3$), magnesite ($MgCO_3$), and ankerite ($FeCO_3$). Iron substitution as well as Mg substitution greater than ~10 mol% will lead to disordering and expansion of the unit cell (Antao et al. 2004; Carmichael and Ferry 2008). These disordered phases are thermodynamically metastable and over time, and with diagenetic alteration, through dissolution/re-precipitation are replaced by more ordered phases.

Dolomite stoichiometry can be measured using atomic absorption spectroscopy, inductively coupled plasma, and electron microprobe. Crystal structure and ordering of dolomite can be identified using X-ray diffraction (XRD) techniques; however, determination of stoichiometry requires the use of empirical curves that relate dolomite to calcite d_{104} to account for unit cell changes with substitution of $MgCO_3$ (e.g., Zhang et al. 2010). In mixed mineralogy samples and in samples where dolomite is in low abundance, XRD may not give unequivocal results of stoichiometry and ordering (e.g., Gregg et al. 2015), and techniques such as transmission electron microscopy (Fig. 1) with selected area electron diffraction (Zhang et al. 2010; Zhang et al. 2012a; Zhang et al. 2012b; Roberts et al. 2013), laser scanning Raman spectroscopy (e.g., Sun et al. 2014), synchrotron-based energy-dispersive X-ray diffraction, and infrared spectroscopy (Rodriguez-Blanco et al. 2015) may help confirm these results.

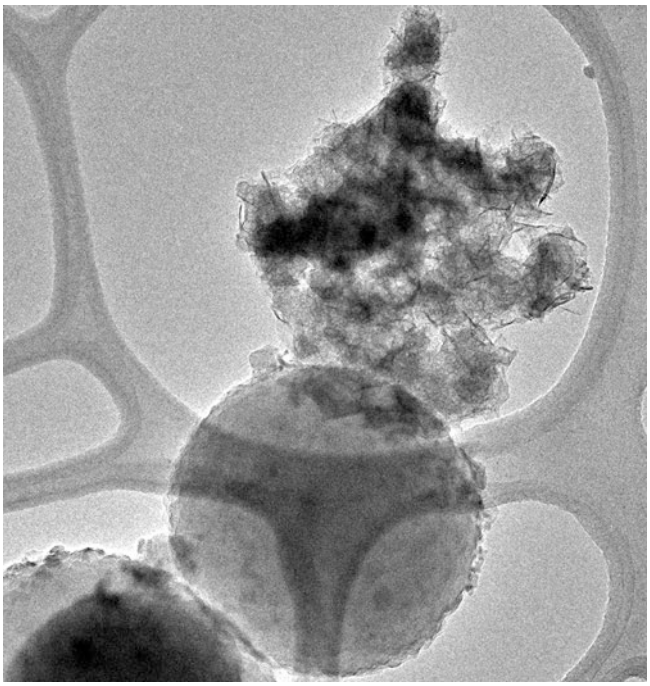

Dolomite and Dolomitization, Fig. 1 Dolomite precipitates abiotically at 25 °C on a carboxylated, polystyrene sphere in seawater approximating Silurian conditions (see Roberts et al. 2013 for experimental conditions). Sphere is 0.8 μm in diameter

Kinetics of Precipitation

Stoichiometric, ordered dolomite readily forms at temperatures above 100 °C (Arvidson and Mackenzie 1999); however, changes in temperature and solution chemistry significantly influence the stoichiometry of precipitated phases. Thermodynamic constants and isotopic fractionation factors have been developed for dolomite at high temperatures (80–250 °C; Baker and Kastner 1981; Sibley et al. 1987; Li et al. 2015) and extrapolated to lower temperatures where laboratory synthesis is hindered by slow reaction kinetics (e.g., Land 1998). Kinetic inhibition of dolomite precipitation at low temperature is attributed to lack of persistent solution supersaturation, low Mg:Ca ratios, sulfate inhibition, Mg-dehydration barrier, and lack of nucleation sites or critical nuclei (e.g., Baker and Kastner 1981; Hardie 1987; Zhong and Mucci 1989; Slaughter and Hill 1991; Brady et al. 1996; Arvidson and Mackenzie 1999; Wright and Wacey 2004).

There are many reports of microbially facilitated dolomite at low temperature (<80 °C) in which kinetic barriers such as solution supersaturation, sulfate inhibition, Mg desolvation, and nucleation sites are attributed to microbial metabolism and surfaces (e.g., Vasconcelos et al. 1995; Warthmann et al. 2000; Mazullo 2000; van Lith et al. 2003; Moreira et al. 2004; Roberts et al. 2004; Wright and Wacey 2004; Wright and Wacey 2005; Braissant et al. 2007; Bontognali et al. 2008; Sánchez-Román et al. 2008; Sánchez-Román et al. 2009; Kenward et al. 2009; Bontognali et al. 2010; Krause et al. 2012; Kenward et al. 2013; Meister et al. 2007; Petrash et al. 2015). These reports link microorganisms to dolomite formation; however, few studies have identified definitive mechanisms by which microbial activity or surfaces facilitate nucleation and subsequent precipitation at low temperature. Enhanced Mg incorporation into the calcite crystal structure has been linked abiotically to dissolved sulfide, which sorbs onto crystal surfaces and facilitates Mg dehydration (Zhang et al. 2012b). Dolomite and Mg-calcite precipitation has been linked also to exopolymeric substances found in microbial biofilms (Bontognali et al. 2008; Krause et al. 2012) in which carboxyl groups associated with these surfaces or other organic matter complex and dehydrate Mg (e.g., Zhang et al. 2012a; Roberts et al. 2013). Many of these reports are of disordered phases, although there are reports of ordered, stoichiometric dolomite forming at low temperature (e.g., Roberts et al. 2004; Kenward et al. 2009; Kenward et al. 2013; Roberts et al. 2013).

Geological Significance and Occurrence

A long-standing conundrum in the geosciences is the so-called dolomite problem. Modern dolomite is scarce and rarely forms on Earth today due to slow reaction kinetics (<50 °C); however, ancient low-temperature dolomite formed in large quantities in Precambrian oceans and throughout the Phanerozoic from so-called calcite seas, apparently dependent upon secular variation of seawater geochemistry (Hardie 1987). Temporal changes in seawater Mg:Ca ratios, pCO_2, and dissolved sulfate concentrations contribute to thermodynamic favorability of aragonite ($CaCO_3$) versus calcite ($CaCO_3$) and dolomite (Wilkinson and Given 1986). Ancient dolomite formed through both primary precipitation and replacement (dolomitization) of $CaCO_3$, presumably by Mg-rich fluids. In modern systems, primary dolomite is constrained to hypersaline environments, such as lagoons (e.g., Vasconcelos and McKenzie 1997) and sabkha environments (e.g., Wright and Wacey 2005), and evidence of ongoing dolomitization of $CaCO_3$ in low-temperature settings has not been reported.

Large-scale models of carbonate dolomitization, including mixing of seawater and groundwater, reflux dolomitization by mesohaline brines, and (hydro)thermal circulation of seawater, have varying evidence of their contributions to dolomitization (e.g., Machel 2004). These models underpin the prevalence of dolomite as a prolific petroleum reservoir. Its utility as a reservoir is attributed to the fact that dolomite preserves its porosity more readily with burial than other carbonate units (Schmoker and Halley 1982; Sun 1995) due to the increased resistance to mechanical and chemical compaction of dolomite compared to calcite (Gale et al. 2010).

History and Use

Giovanni Arduino, an Italian geologist, is credited with the first identification of the mineral now known as dolomite in 1779 (McKenzie and Vasconcelos 2009); however, Déodat de Dolomieu is credited with recognizing the mineral that makes up the mountains now known as the Dolomite Mountains of Northern Italy (de Dolomieu 1791; Zenger et al. 1994).

In addition to its utility as a petroleum reservoir, dolomite is also used as a paleothermometer and a tracer of seawater geochemistry. It is mined and used as a source of Mg and a pH buffer in soils and is used as a flux for smelting and ceramics.

Summary

Extensive research has been performed on kinetics of dolomite precipitation and dolomitization reactions. These efforts further refine models of large-scale dolomite formation that are found in ancient rock.

Cross-References

- ▶ Calcium
- ▶ Carbonate Compensation Depth
- ▶ Crystal Chemistry
- ▶ Diagenesis
- ▶ Fluid–Rock Interaction
- ▶ Kinetics of Geochemical Processes
- ▶ Low-Temperature Geochemistry
- ▶ Magnesium
- ▶ Mineralogy
- ▶ Ocean Biochemical Cycling and Trace Elements
- ▶ Petroleum

References

Antao S, Mulder W, Hassan I, Crichton W, Parise J (2004) Cation disorder in dolomite, $CaMg(CO_3)_2$, and its influence on the aragonite + magnesite ↔ dolomite reaction boundary. Am Mineral 89:1142–1147

Arvidson R, MacKenzie F (1999) The dolomite problem: control of precipitation kinetics by temperature and saturation state. Am J Sci 299:257–288

Baker P, Kastner M (1981) Constraints on the formation of sedimentary dolomite. Science 213:214–216

Bontognali T, Vasconcelos C, Warthmann R, Dupraz C, Bernasconi S, McKenzie J (2008) Microbes produce nanobacteria-like structures, avoiding cell entombment. Geology 36:663–666

Bontognali T, Vasconcelos C, Warthmann R, Bernasconi S, Dupraz C, Strohmenger C, McKenzie J (2010) Dolomite formation within microbial mats in the coastal sabkha of Abu Dhabi (United Arab Emirates). Sedimentology 57:824–844

Brady P, Krumhans J, Papenguth J (1996) Surface complexation clues to dolomite growth. Geochim Cosmochim Acta 60:727–731

Braissant O, Decho W, Dupraz C, Glunk C, Przekop K, Visscher P (2007) Exopolymeric substances of sulfate-reducing bacteria: interactions with calcium at alkaline pH and implication for formation of carbonate minerals. Geobiology 5:401–411

Carmichael S, Ferry A (2008) Formation of replacement dolomite in the latemar carbonate buildup, dolomite, Northern Italy: part 2. Origin of the dolomitization fluid and the amount and duration of fluid flow. Am J Sci 308:885–904

de Dolomieu D (1791) Sur un genre de pierres calcaires trespeu effervescentes avec les acides et phosphorescentes par la collision. J Phys 39:3–10

Gale J, Lander R, Reed F, Laubach S (2010) Modeling fracture porosity evolution in dolostone. J Struct Geol 32:1201–1211

Gregg J, Bish D, Kaczmarek S, Machel H (2015) Mineralogy, nucleation and growth of dolomite in the laboratory and sedimentary environment: a review. Sedimentology 62:1749–1769

Hardie L (1987) Dolomitization: a critical view of some current views. J Sediment Petrol 57:166–183

Kenward P, Goldstein R, González L, Roberts J (2009) Precipitation of low-temperature dolomite from an anaerobic microbial consortium: the role of methanogenic Archaea. Geobiology 7:556–565

Kenward P, Goldstein R, González L, Fowle D, Ueshima M, Roberts J (2013) Ordered, low-temperature dolomite mediated by carboxyl-group density of microbial cell walls. AAPG Bull 97:2113–2125

Krause S, Liebtrau V, Gorb S, Sanchez-Roman M, McKenzie M, Treude T (2012) Microbial nucleation of Mg-rich dolomite in exopolymeric substances under anoxic modern seawater salinity: new insight into an old enigma. Geology 40:587–590

Land L (1998) Failure to precipitate dolomite at 25°C from dilute solution despite 1000-fold oversaturation after 32 years. Aquat Geochem 4:361–368

Li W, Beard BL, Li C, Xu H, Johnson C (2015) Experimental calibration of Mg isotope fractionation between dolomite and aqueous solution and its geological implications. Geochim Cosmochim Acta 157:164–181

Machel H (2004) Concepts and models of dolomitization: a critical reappraisal. Geol Soc Lond, Spec Publ 235:7–63

Mazullo S (2000) Organogenic dolomitization in peritidal to deep sea sediments. J Sediment Res 70:10–23

McKenzie J, Vasconcelos C (2009) Dolomite Mountains and the origin of the dolomite rock of which they mainly consist: historical developments and new perspectives. Sedimentology 56:205–219

Meister P, McKenzie J, Vasconcelos C, Bernasconi S, Frank M, Guthjahrs M, Schrag M (2007) Dolomite formation in the dynamic deep biosphere: results from the Peru margin. Sedimentology 54:1007–1031

Moreira N, Walter W, Vasconcelos C, McKenzie J, McCall P (2004) Role of sulfide oxidation in dolomitization: sediment and pore-water geochemistry of a modern hypersaline lagoon system. Geology 32:701–704

Petrash D, Lalonde S, Gonzalez-Arismendi G, Gordon R, Gingras M, Konhauser K (2015) Can Mn-S cycling drive sedimentary dolomite formation? A hypothesis. Chem Geol 404:27–40

Reeder R, Wenk H (1983) Structure refinements of some thermally disordered dolomites. Am Mineral 68:769–776

Roberts J, Bennett P, Macpherson G, González L, Milliken K (2004) Microbial precipitation of dolomite in groundwater: field and laboratory experiments. Geology 32:277–280

Roberts J, Kenward P, Fowle D, González L, Goldstein R, Moore D (2013) Surface chemistry allows for precipitation of dolomite at low temperature. PNAS 110:14540–14545

Rodriguez-Blanco J, Shaw S, Benning L (2015) A route for the direct crystallization of dolomite. Am Mineral 100:1172–1181

Sánchez-Román M, Vasconcelos C, Schmid T, Dittrich M, McKenzie J, Zenobi R, Rivadeneyra M (2008) Aerobic microbial dolomite at the nanometer scale: implications for the geologic record. Geology 36:879–882

Sánchez-Román M, McKenzie J, de Luca Rebello Wagner A, Rivadeneyra M, Vasconcelos C (2009) Presence of sulfate does not inhibit low-temperature dolomite precipitation. Earth Planet Sci Lett 285:131–139

Schmoker J, Halley R (1982) Carbonate porosity versus depth: a predictable relation for South Florida. AAPG Bull 66:2561–2570

Sibley D, Dedoes R, Bartlett T (1987) The kinetics of dolomitization. Geology 15:1112–1114

Slaughter M, Hill R (1991) The influence of organic matter in organogenic dolomitization. J Sediment Petrol 61:296–303

Sun S (1995) Dolomite reservoirs: porosity evolution and reservoir characteristics. AAPG Bull 79:186–204

Sun J, Wu Z, Cheng H, Zhang Z, Frost R (2014) A Raman spectroscopic comparison of calcite and dolomite. Spectrochim Acta A Mol Biomol Spectrosc 117:158–162

van Lith Y, Warthmann R, Vasconcelos C, McKenzie J (2003) Sulfate-reducing bacteria induce low-temperature Ca dolomite and high-Mg calcite formation. Geobiology 1:71–79

Vasconcelos C, McKenzie J (1997) Microbial mediation of modern dolomite precipitation and diagenesis under anoxic conditions

(Lagoa Vermelha, Rio de Janeiro, Brazil). J Sediment Res 67:378–390
Vasconcelos C, McKenzie J, Bernasconi S, Grujic D, Tien A (1995) Microbial mediation as a possible mechanism for natural dolomite formation at low temperatures. Nature 377:220–222
Warthmann R, van Lith Y, Vasconcelos C, McKenzie J, Karpoff A (2000) Bacterially induced dolomite precipitation in anoxic culture experiments. Geology 28:1091–1094
Wilkinson B, Given K (1986) Secular variation in abiotic marine carbonates: constraints on Phanerozoic atmospheric carbon dioxide contents and oceanic Mg/Ca ratios. J Geol 94:21–33
Wright D, Wacey D (2004) Sedimentary dolomite: a reality check. In: Braithwaite C, Rizzi G, Darke G (eds) The geometry and petrogenesis of dolomite hydrocarbon reservoirs, Special publication, vol 235. Geological Society, pp 65–74
Wright D, Wacey D (2005) Precipitation of dolomite using sulfate-reducing bacteria from the Coorong region, South Australia: significance and implications. Sedimentology 28:987–1008
Zenger D, Bourrouilh-Le Jan F, Carozzi A (1994) Dolomieu and the first description of dolomite. In: Purser B, Tucker M, Zenger D (eds) Dolomites: a volume in honour of dolomieu, IAS special publication, vol 21, New York, pp 21–28
Zhang F, Xu H, Konishi H, Roden E (2010) A relationship between d104 value and composition in the calcite-disordered dolomite solid-solution series. Am Mineral 95:1650–1656
Zhang F, Xu H, Konishi H, Shelobolina E, Roden E (2012a) Polysaccharide-catalyzed nucleation and growth of disordered dolomite: a potential precursor of sedimentary dolomite. Am Mineral 97:556–567
Zhang F, Xu H, Konishi H, Kemp J, Roden E (2012b) Dissolved sulfide-catalyzed crystallization of Ca-Mg carbonates and implications for the formation mechanism of sedimentary dolomite. Geochim Cosmochim Acta 97:148–165
Zhong S, Mucci A (1989) Calcite and aragonite precipitation from seawater solutions of various salinities: precipitation rates and overgrowth compositions. Chem Geol 78:283–299

Dysprosium

Scott M. McLennan
Department of Geosciences, Stony Brook University, Stony Brook, NY, USA

Element Data
Atomic Symbol: Dy
Atomic Number: 66
Atomic Weight: 162.500(1)
Isotopes and Abundances: ^{156}Dy, 0.056(3)%; ^{158}Dy, 0.095(3)%; ^{160}Dy, 2.329(18)%; ^{161}Dy, 18.889(42)%; ^{162}Dy, 25.475(36)%; ^{163}Dy, 24.896(42)%; and ^{164}Dy, 28.260(54)%
1 Atm Melting Point: 1412 °C
(*continued*)

1 Atm Boiling Point: 2567 °C
Common Valences: +3
Ionic Radii: 91.2 pm (CN6), 102.7 pm (CN8), and 122.8 pm (CN12)
Pauling Electronegativity: 1.22
First Ionization Energy: 573.02 kJ mol^{-1}
Chondritic (CI) Abundance: 0.254 ppm
Silicate Earth Abundance: 0.566 ppm
Crustal Abundance: 3.7 ppm
Seawater Abundance: 1.06 ppt
Core Abundance: ~0

Properties

Dysprosium (Dy), from the Greek *dysprositos* (hard to access), is a soft, ductile, dense (8.551 g cm^{-3}), bright silvery metal. Its electronic configuration is [Xe]4f^{10}6s^{2}. It is stable at room temperature and readily dissolves in mineral acids. It is a group 3 or IIIB inner transition element, with +3 being its only valence state in geological environments, and is one of the lanthanide rare earth elements (REE). In geochemical terminology, it is grouped with heavy rare earth elements (HREE; Gd-Lu). Dysprosium has seven natural, stable isotopes, listed above with their abundances.

More than 270 minerals contain lanthanides as essential structural constituents, but those with Dy as a major component are restricted to Y and HREE varieties, such as xenotime [$Y(PO_4)$], bastnäsite [$REE(CO_3)F$], allanite [$(REE,Ca,Y)_2(Al,Fe^{2+},Fe^{3+})_3(SiO_4)_3(OH)$], and britholite [$(REE,Ca)_5(SiO_4,PO_4)_3(OH,F)$]. In addition, Dy may be enriched in ion adsorption lateritic kaolinite–halloysite clay deposits that are mined for REE.

Details of properties, mineralogy, history, and uses of Dy were compiled from Goonan (2011), Chakhmouradian and Wall (2012), Zaimes et al. (2015), Gschneidner Jr (2016), Hammond (2016), and Meija et al. (2016a, b).

History and Use

Dysprosium was discovered in 1886 by Paul Émile Lecoq de Boisbaudran but not isolated until about 1950. Its major use is as a component for neodymium magnets. Due to a relatively high thermal absorption cross section, Dy_2O_3–nickel ceramic metals (cermets) have been used in nuclear reactor cooling rods. Other uses include as components in lasers, magnets, metallic coatings, ionizing radiation dosimeters, transducers, and infrared radiation sources.

Geochemical Behavior

The fundamental importance of Dy in geochemistry is that it is one of the small trivalent rare earth elements, among the most useful trace elements in all areas of geochemistry and cosmochemistry due to their coherent and systematic behavior as a group, largely a consequence of the "lanthanide contraction."

Dysprosium is typically a trace element in most rocks and minerals. It is classified geochemically and cosmochemically as a highly refractory lithophile element with a 50% $T_{condensation}$ of 1659 K at 10^{-4} bars (Lodders 2003). In most igneous systems, Dy is incompatible with bulk partition coefficients, $D < 1$. In aqueous systems, Dy normally has very low fluid/rock partition coefficients ($\ll 1$). As a result, Dy contents of clastic sediments typically reflect their average provenance abundances.

In seawater, Dy has very low concentrations (~ppt) and residence times (~740 year) with speciation dominated by Dy^{3+}, $DyCO_3^+$, and $Dy(CO_3)_2^-$. In other aqueous systems (e.g., magmatic, hydrothermal), Dy can reach ppm levels due to elevated temperatures, pH effects, and complexing with various ligands (e.g., F^-, Cl^-, OH^-).

Concentration and residence time data are from compilations in Taylor and McLennan (2009) and Nozaki (2001).

Biological Utilization and Toxicity

There are no documented biological uses for Dy, but in China REE have been added to fertilizers and to stock feed to promote growth. REE (including Dy^{3+}) likely substitute for Ca^{2+} in biological materials and processes. REE concentrations (including Dy) in human tissues and fluids are very low (tens of ppb to <ppb levels, respectively) due to very low concentrations in natural waters and low uptake rates throughout the food chain (Bulman 2003). At low levels of ingestion, there are no established toxic effects that pose a threat to human health.

Cross-References

- Incompatible Elements
- Lanthanide Rare Earths
- Lithophile Elements
- Trace Elements
- Transition Elements

References

Bulman RA (2003) Metabolism and toxicity of the lanthanides. In: Sigel A, Sigel H (eds) Metal ions in biological systems, Vol. 40, the lanthanides and their interrelations and Biosystems. Marcel Dekker, Basel, pp 683–703

Chakhmouradian AR, Wall F (2012) Rare earth elements. Elements 8:333–376

Goonan TG (2011) Rare earth elements – end use and recyclability. US Geol Surv Sci Invest Rpt 2011–5094. 15pp

Gschneidner KA Jr (2016) Physical properties of the rare earth metals. In: Haynes WM (ed) CRC handbook of chemistry and physics, 96th edn. CRC Press, Boca Raton, pp 4-115–4-120

Hammond CR (2016) The elements. In: Haynes WM (ed) CRC handbook of chemistry and physics, 96th edn. CRC Press, Boca Raton, pp 4-1–4-42

Lodders K (2003) Solar system abundances and condensation temperatures of the elements. Astrophys J 591:1220–1247

Meija J, Coplen TB, Berglund M, Brand WA, De Bièvre P, Gröning M, Holden NE, Irrgeher J, Loss RD, Walczyk T, Prohaska T (2016a) Atomic weights of the elements 2013. Pure Appl Chem 88:265–291. (IUPAC Technical Report)

Meija J, Coplen TB, Berglund M, Brand WA, De Bièvre P, Gröning M, Holden NE, Irrgeher J, Loss RD, Walczyk T, Prohaska T (2016b) Isotopic compositions of the elements 2013. Pure Appl Chem 88:293–306. (IUPAC Technical Report)

Nozaki Y (2001) Rare earth elements and their isotopes in the ocean. In: Steele JH et al (eds) Encyclopedia of ocean sciences. Academic, London, pp 2354–2366

Taylor SR, McLennan SM (2009) Planetary crusts: their composition, origin and evolution. Cambridge University Press, Cambridge. 378 pp

Zaimes GG, Hubler BJ, Wang S, Khanna V (2015) Environmental life cycle perspective on rare earth oxide production. ACS Sustain Chem Eng 3:237–244